Published in final edited form as:

Biochemistry. 2019 March 05; 58(9): 1246–1259. doi:10.1021/acs.biochem.9b00041.

Transition State Analysis of the Reaction Catalyzed by the Phosphotriesterase from *Sphingobium* sp. TCM1

Andrew N. Bigley[δ], **Dao Feng Xiang**[δ], **Tamari Narindoshvili**[δ], **Charlie W. Burgert**[Ψ], **Alvan C. Hengge**[Ψ], **Frank M. Raushel**[δ]

[δ]Department of Chemistry, Texas A&M University, College Station TX 77843, United States

[Ψ]Department of Chemistry and Biochemistry, Utah State University, Logan UT 84322, United States

Abstract

Organophosphorus flame-retardants are stable toxic compounds used in nearly all durable plastic products and are considered major emerging pollutants. The phosphotriesterase from *Sphingobium* sp. TCM1 (*Sb*-PTE) is one of the few enzymes known to be able to hydrolyze organophosphorus flame-retardants such as triphenyl phosphate and tris(2-chloroethyl) phosphate. The effectiveness of *Sb*-PTE for the hydrolysis of these organophosphates appears to arise from its ability to hydrolyze unactivated alkyl and phenolic esters from the central phosphorus core. How *Sb*-PTE is able to catalyze the hydrolysis of the unactivated substituents is not known. To interrogate the catalytic hydrolysis mechanism of *Sb*-PTE, the pH-dependence of the reaction and the effects of changing the solvent viscosity were determined. These experiments were complemented by measurement of the primary and secondary 18-oxygen isotope effects on substrate hydrolysis and a determination of the effects of changing the pK_a of the leaving group on the magnitude of the rate constants for hydrolysis. Collectively, the results indicated that a single group must be ionized for nucleophilic attack and that a separate general acid is not involved in protonation of the leaving group. The Brønsted analysis and the heavy atom kinetic isotope effects are consistent with an early associative transition state with subsequent proton transfers not being rate limiting. A novel binding mode of the substrate to the binuclear metal center and a catalytic mechanism are proposed to explain the unusual ability of *Sb*-PTE to hydrolyze unactivated esters from a wide range of organophosphate substrates.

Graphical Abstract:

Corresponding Authors: Frank M. Raushel; raushel@tamu.edu, Alvan Hengge; alvan.hengge@usu.edu.

Notes

The authors declare no competing financial interest.

Accession code: *Pd*-PTE, A0A077JBW9

Supporting Information

Physical constant for synthesized compounds, corrections for isotopic ratios used for heavy atom isotope effects, and additional NMR data.

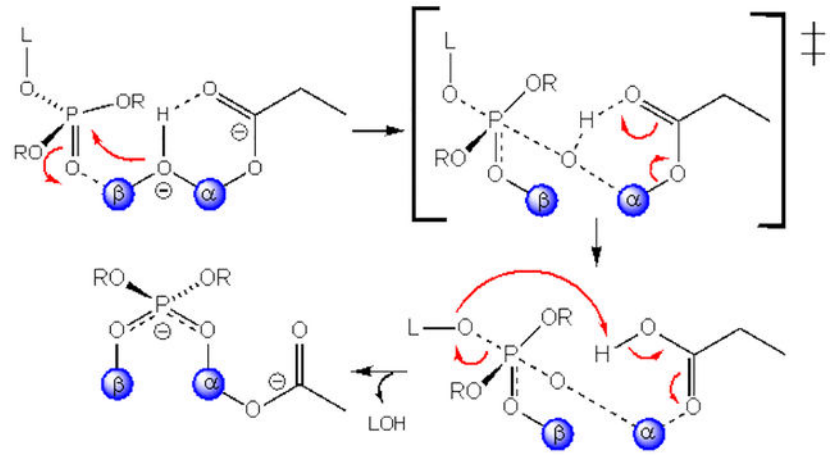

INTRODUCTION

The phosphotriesterase from *Sphingobium* sp. TCM1 (*Sb*-PTE) is unique among phosphotriesterase enzymes in that it will hydrolyze organophosphate flame-retardants and plasticizers.[1, 2] Unlike the better-known organophosphate nerve agents, the organophosphate flame-retardants lack the typical labile leaving group, which gives rise to the neurotoxicity of the nerve agents.[3] These compounds are commonly used in plastics and foams and are produced at rates of hundreds of tons per year.[4] While not neurotoxins, organophosphate flame-retardants have been noted as potential carcinogens and are developmental toxins in animal and human models.[5–7] The widespread use of these compounds has led them to be considered as major emerging pollutants with widespread contamination of soil, water, and air.[4, 8]

The potential to utilize *Sb*-PTE for bioremediation of organophosphorus flame retardants has encouraged efforts to characterize the enzymatic activity of this enzyme.[1, 2] The structure of *Sb*-PTE was recently determined to have a 7-bladed β-propeller protein fold with a binuclear Mn^{+2} metal center embedded at the top of the central core of the enzyme (Figure 1).[9] The substrate binding site is found directly above and essentially perpendicular to the plane of the metal center.

Sb-PTE has been shown to catalyze the hydrolysis of phosphotriesters via a direct nucleophilic attack of hydroxide (or water) on the phosphorus of the bound substrate.[10] It is highly probable that the nucleophilic water is initially coordinated by the two divalent cations bound in the active site of enzyme.[9] However, other phosphotriesterase enzymes generally exhibit a very strong dependence on the pK_a of the leaving group.[11–13] For example, the phosphotriesterase from *Pseudomonas diminuta* (*Pd*-PTE) has a 100,000-fold reduction in catalytic activity when *p*-nitrophenol is substituted with phenol as the leaving group.[14] With *Sb*-PTE, there is only ~2-fold difference in the rate of hydrolysis between dibutyl *p*-nitrophenyl phosphate and dibutyl phenyl phosphate.[2] One simple explanation is that *Sb*-PTE effectively delivers a proton to the leaving group during the course of the reaction, but how that proton might be delivered is unclear. Further complicating the study of *Sb*-PTE is the observation that this enzyme can hydrolyze any one of the three ester bonds

within a given substrate resulting in multiple reaction products.[15] However, the ability to cleave a simple alkyl ester leaving group appears to require at least one other substituent attached to the central phosphorus core with a pK_a <11. With some substrates the hydrolysis of a methyl ester can proceed at the same rate as hydrolysis of a *p*-nitrophenyl ester within the same compound.[15] How *Sb*-PTE is able to catalyze the hydrolysis of simple alkyl esters at the same rate as an activated phenolate ester has yet to be determined.

As an initial probe of the activation mechanism for the nucleophilic water molecule and to test the potential of additional groups within the active site that may function as a general acid for the direct protonation of the leaving group, the pH-rate profile of *Sb*-PTE was obtained. The degree of charge development in the transition state during substrate hydrolysis was addressed by a systematic variation of the pK_a of the leaving group ester, and by kinetic isotope effects in the leaving group and in the nonbridging oxygen positions of the substrate paraoxon. The rate limiting steps during product formation were probed by measuring the effects of solvent viscosity and the substitution of D_2O for H_2O during enzyme-catalyzed hydrolysis of the substrate paraoxon.

MATERIALS and METHODS

Materials.

Unless otherwise stated, the bacterial growth medium was purchased from Research Products International and general chemicals were obtained from Sigma/Aldrich. Paraoxon (**5**) and tributyl phosphate (**27**) were purchased from Sigma/Aldrich (Scheme 1). DNA sequencing was conducted by Eton Biosciences Inc. Compounds **19–27** were synthesized by previously reported methods.[2]

Chemical Synthesis of Substrates.

Phosphotriesters **1**-**5** and **7**-**18** were synthesized with modifications of previously published methods.[11] For compounds **1–5**, **7**-**11**, and **13–18** a stirred reaction mixture containing 5 mmol phenol (or substituted phenol) and 6 mmol of triethylamine in 20 mL of anhydrous dichloromethane was cooled to 0 °C and diethyl chlorophosphate (97%, 6 mmol) added dropwise. The reaction was allowed to warm to ambient temperature (23 °C) and then stirred for an additional 18 h. The reaction was quenched by the addition of 2.0 mL of water. The organic phase was washed with 0.1 N HCl and saturated $NaHCO_3$, dried over $NaSO_4$, and then the solvent was removed by rotary evaporation. The product was purified by silica gel chromatography (hexanes: EtOAc mixtures) yielding pure compounds in yields of 42 – 65%. The physical constants are provided in the Supplementary Information.

For compound **12**, diethyl chlorophosphate (0.29 mL, 97%, 2 mmol) was added dropwise to a stirred reaction mixture of 4-hydroxybenzamide (0. 27 g, 2 mmol) and K_2CO_3 (0.28 g, 2 mmol) in 7.0 mL of anhydrous tetrahydrofuran. The reaction was stirred for 24 h, filtered, and then 20 mL of EtOAc were added. The organic phase was washed with 0.1 N HCl and saturated $NaHCO_3$ solution, dried over $NaSO_4$, and the solvent removed by rotary evaporation. The residue was purified by silica gel chromatography (EtOAc:MeOH, 20:1), yielding 100 mg (19%) of a white solid product. Organophosphate triesters are potentially

toxic and thus the appropriate safety precautions must be used when handling these compounds. The structures of the substrates used for this investigation are presented in Scheme 1.

Expression and Purification of *Sb*-PTE.

The gene for wild-type *Sb*-PTE (gi|664819019; UniProt id: A0A077JBW9) was cloned into a pET30a(+) plasmid using a codon optimized sequence to enable expression of the C-terminal histidine-tagged *Sb*-PTE as previously described.[2] The plasmid was transformed into *E. coli* BL21(DE3) cells (EMD Millipore), and single colonies were used to inoculate 6-mL cultures of LB medium, which were grown for 8 h at 37 °C. The 6-mL cultures were subsequently used to inoculate 1-L cultures of Terrific Broth, supplemented with 1.0 mM $MnAc_2$ and then grown at 27 °C for 20 h. The cells were harvested by centrifugation and stored at −80 °C. Frozen cell pellets (~10 g) were resuspended in 50 mL of binding buffer (20 mM HEPES, pH 7.9, 0.5 M NaCl, and 10 mM imidazole). Following the disruption of cells by sonication using a Branson Sonifier 450, the solution was clarified by centrifugation (15,300 × g for 20 min). The supernatant solution was passed through a 0.45 μm syringe filter and subjected to Ni-affinity chromatography using a 5-mL HisTrap FF column (GE Healthcare) attached to an NGC liquid chromatography system (Bio-Rad) previously equilibrated with binding buffer. The column was washed with 30 column volumes of binding buffer, and then *Sb*-PTE was eluted with a linear gradient of 10 – 250 mM imidazole. The fractions with paraoxonase activity were combined and concentrated. The elution buffer was exchanged with 20 mM HEPES, pH 8.0, containing 100 mM NaCl, using a PD-10 desalting column (GE Healthcare). The protein purity was judged to be >95% by SDS-PAGE using a Mini-PROTEIN TGX Gels (Bio-Rad). The yield of *Sb*-PTE was ~10 mg/L of cell culture.

Determination of Extinction Coefficients.

Extinction coefficients for hydrolysis of the modified phenolic groups from compounds **1–21** were determined at either pH 9.0 or 10.0. Generally, solutions of the substituted phenol were prepared in methanol and then diluted in the appropriate buffer with a final concentration of 10% MeOH. The UV spectra were recorded using a 1-cm quartz cuvette and the spectra of an identical concentration of the corresponding phosphotriesters were recorded in the same cuvette. The substrate spectrum was subtracted from the spectrum of the substituted phenol to generate a difference spectrum, which was used to identify the optimal wavelength for the assay and to calculate the appropriate extinction coefficient. The extinction coefficients and the wavelengths use to measure the enzymatic rates of hydrolysis of compounds **1- 21** are listed in Table S1.

Optimization of Catalytic Activity.

The catalytic activity of *Sb*-PTE was tested with various buffers using 1.0 mM paraoxon (**5**) as the substrate. The buffers HEPES, TRIS, CHES, BICINE, TRICINE, Gly-Gly, TAPS, TABS, and AMPSO were each tested at a concentration of 50 mM at pH 8.5. Each buffer was subsequently tested in the presence of 20 – 500 mM of each of the following salts: NaCl, KCl, NH_4Cl, or $(NH_4)_2SO_4$ using 1.0 mM paraoxon (**5**) as the substrate.

pH-Rate Profile.

The kinetic constants, k_{cat} and k_{cat}/K_m, were measured for *Sb*-PTE using paraoxon (**5**) or diethyl phenyl phosphate (**17**) as the substrate at pH values ranging from 5.5 to 10.5 at 30 °C. A buffer system consisting of 40 mM MOPS, 40 mM MES, 40 mM HEPES, 40 mM CHES, and 100 mM NH_4Cl (combination buffer) was used for measurement at all pH values. Stock buffer solutions (10×) were adjusted to the appropriate pH prior to dilution. In each case, the reported pH was the measured value at the end of the enzymatic reaction.

Brønsted Analysis.

All kinetic measurements were conducted using a Molecular Devices SpectraMax 384 Plus 96-well plate reader at 30 °C in 250 μL assay mixtures. Combination buffer was used for the experiments at pH 10 for compounds **1–11** and **13-21**. Hydrolysis of compound **12** was followed in the same buffer at pH 9.0. Compounds with diethyl phosphorus centers (**1**-**18**) included a final concentration of 5% methanol as a cosolvent while the dibutyl series (**19**-**27**) used 5% DMSO. For the hydrolysis of 1.0 mM paraoxon by *Sb*-PTE, the inclusion of 5% methanol in the assay reduces the rate of hydrolysis by approximately 30%, while the inclusion of 5% DMSO reduces the rate of hydrolysis by approximately 10%. Hydrolysis of compound **22** was measured by monitoring the release of 1-butanethiol by the inclusion of 0.3 mM DTNB at pH 8.0 (ΔE_{412}= 14 150 M^{-1} cm^{-1}). Hydrolyses of compounds **23**-**27** were monitored using a pH-sensitive colorimetric assay.[16] The reactions were conducted in 2.5 mM BICINE buffer, pH 8.3, containing 0.2 M NaCl, 10% DMSO, and 0.1 mM of the pH indicator cresol purple to monitor proton release from the hydrolysis reaction. The effective extinction coefficient (ΔOD/M of H^+) was found to be $\Delta E_{577} = 1.68 \times 10^3$ M^{-1} cm^{-1} by titration with acetic acid at pH 8.3, 30 °C.

Product Ratios.

^{31}P-NMR spectroscopy was used to assess the composition of the products formed from the hydrolysis of compounds **1**-**27** by *Sb*-PTE. For each assay the substrate was dissolved in DMSO and then diluted to 2.0 mM in a final volume of 1.0 mL containing the combination buffer (pH 10.0) and 5% DMSO. The reactions were initiated by addition of *Sb*-PTE (1–5 μM) and allowed to proceed until the reaction was complete. Enzyme was removed via utrafiltration using a Vivaspin 500 10 kDa MWCO centrifugal device (GE Healthcare). 100 μL D_2O and 50 μL of 100 mM EDTA were added to 650 μL of the reaction mixture prior to the ^{31}P-NMR spectrum being recorded.

To determine if there is a pH-dependence to the product ratios, assays with diethyl phenyl phosphate (**17**) were conducted at pH 7.0, 8.0, 9.0, and 10.0. Reactions containing 0.1 μM *Sb*-PTE, 2.0 mM compound **17**, combination buffer, and 20% methanol were incubated at room temperature until the reaction was complete. Enzyme was removed by centrifugation using a Vivaspin 500 10 kDa MWCO centrifugal device. 100 μL of D_2O and 50 μL of 100 mM EDTA were added to 650 μL of the original reaction mixture before recording the ^{31}P-NMR spectrum.

To determine if there is a concentration dependence to the product ratios, total hydrolysis reactions were conducted using 2.0 mM, 0.5 mM and 10 μM concentrations of diethyl *m*-

fluorophenyl phosphate (**14**). The 2.0 mM reaction was conducted in a volume of 1.0 mL in combination buffer at pH 10. The 0.5 mM reaction was conducted in a volume of 4.0 mL, and the 10 μM reaction was in a total volume of 50 mL. Reactions were initiated by addition of 0.1 μM *Sb*-PTE and incubated at room temperature until the reaction was complete. The 0.5 mM and 10 μM reaction mixtures were concentrated to approximately 1.0 mL under reduced pressure, and the enzyme removed by ultrafiltration using a Vivaspin 500 10 kDa MWCO centrifugal device. 100 μL of D_2O and 50 μL of 100 mM EDTA at pH 10 were added to 650 μL of the original reaction mixture before recording the ^{31}P-NMR spectrum.

Viscosity Effects.

Analysis of the effects of solvent viscosity was conducted using sucrose as the viscogen and either 110 μM dibutyl phenyl phosphate (**21**) or 30 μM paraoxon (**5**) as the substrate in total hydrolysis assays. Assays were conducted in a volume of 1.0 mL with the combination buffer to maintain the pH at 10.0. *Sb*-PTE was preincubated with 100 μM $MnCl_2$ and reactions initiated by the addition of 60 or 48 nM *Sb*-PTE for the hydrolysis of dibutyl phenyl phosphate (**21**) and paraoxon (**5**), respectively. Sucrose was added to final concentrations of 2.0, 4.0, 4.64, 5.5, 10.0, 13.3, 15.6, 21.3, 26.7, or 30 (w/w%) giving relative viscosities of 1.01, 1.03, 1.04, 1.07, 1.15, 1.2, 1.4, 1.8, 2.1 and 2.4 as previously reported.[11] The assays with dibutyl phenyl phosphate (**21**) contained a final concentration of 2.5% MeOH while the assays with paraoxon contained 0.25% MeOH.

Solvent Isotope Effects.

Solvent isotope effects were measured using paraoxon (**5**) and diethyl *m*-fluorophenyl phosphate (**14**) as the substrates at pH 8.5 and 9.0. Reactions were conducted using 35 μM paraoxon (**5**) or 200 μM diethyl *m*-fluorophosphate (**14**) in total hydrolysis reactions. Reactions were 1.0 mL total volume with 50 mM CHES and 100 mM NH_4Cl. The pD of D_2O solutions was determined as pD = pH + 0.4 using a standard pH meter calibrated in H_20 buffers.[17] The reactions were initiated by the addition of 48 nM *Sb*-PTE for paraoxon (**5**) or 60 nM for diethyl *m*-fluorophenyl phosphate (**14**) and followed at an appropriate wavelength in a cuvette until the reaction was complete. Reactions were replicated 2 to 5 times and the reported isotope effects are the average obtained from all replicates. The solvent deuterium isotope effect on k_{cat} was measured by determining the steady state reaction kinetics with paraoxon (**5**) at pH 9.0. Reactions were 250 μL total volume with 50 mM CHES, 1.0 mM $MnCl_2$, 100 mM NH_4Cl and 0.001–1.5 mM paraoxon in either H_2O or D_2O. Reactions were initiated by addition of 0.5 μM *Sb*-PTE.

Similar reactions were conducted to determine the solvent isotope effects on the chemical hydrolysis of 35 μM paraoxon (**5**) and 200 μM diethyl *m*-fluorophenyl phosphate (**14**). Substrate stock solutions were made in D_2O with 5% deuterated DMSO. 5 μL of paraoxon or 50 μL of diethyl *m*-fluorophenyl phosphate was diluted into either H_2O or D_2O and hydrolysis initiated by addition of 50 μL of 40% (w/w) KOD (Sigma Aldrich). Reactions were 1.0 mL total volume and followed at the appropriate wavelength until complete.

To evaluate the solvent isotope effect on the product ratio, approximately 2 mg of paraoxon (**5**) or diethyl *m*-fluorophenyl phosphate (**14**) were hydrolyzed to completion in a 1.0 mL

total volume reaction containing 50 mM CHES (pH 8.5), 100 mM NH_4Cl and 5% deuterated DMSO with either H_2O or D_2O as the solvent. Substrates were predissolved in 50 μL of deuterated DMSO. Reactions were initiated by the addition of 1.2 μM *Sb*-PTE. Once the reaction was complete the enzyme was removed by ultrafiltration using a Nanosep 10K Omega (Pall Corporation) centrifugal filtration device. 650 μL of the reaction mixture was added to 100 μL of D_2O and the ^{31}P NMR spectra were recorded.

Data Analysis.

Steady state kinetic parameters for the release of phenols, alcohols and thiols were determined by fitting the initial rates to eqn. 1 using the nonlinear least-squares fitting program in SigmaPlot 10.0, where v in the initial velocity, E_t is the enzyme concentration, k_{cat} is the turnover number, [A] is the substrate concentration and K_m is the Michaelis constant.

$$v/E_t = (k_{cat}[A]/(K_m + [A]) \quad (1)$$

Kinetic constants for the total hydrolysis of substrates by *Sb*-PTE and the rate constants for the release of individual substituents from the various phosphotriester substrates were obtained using equations 2–5, where $^{T}k_{cat}$ and $^{T}(k_{cat}/K_m)$ are the sum of the kinetic constants for the hydrolysis of all leaving groups catalyzed by *Sb*-PTE with a given substrate. $^{1}k_{cat}$ and $^{1}(k_{cat}/K_m)$ are the observed kinetic constants obtained directly from the spectroscopically determined hydrolysis of the phenolate (compounds **1**-**21**) or thiolate ester (compound **22**). F is the fraction of the total product formed from the hydrolysis of the phenolate or thiolate ester as determined from the ^{31}P-NMR analysis of the product ratios. $^{2}k_{cat}$ and $^{2}(k_{cat}/K_m)$ are the rate constants for cleavage of the alcohol substituents by *Sb*-PTE. An analogous approach was utilized for measurement of the kinetic constants for the substituted butyl groups in compounds **23**-**27**, except the observed rates correspond to the total hydrolysis and each component is the obtained by multiplying its fractional hydrolysis times the total value.

$$^{T}k_{cat} = {}^{1}k_{cat}/F \quad (2)$$

$$^{T}(k_{cat}/K_m) = {}^{1}(k_{cat}/K_m)/F \quad (3)$$

$$^{T}k_{cat} = {}^{1}k_{cat} + {}^{2}k_{cat} \quad (4)$$

$$^{T}(k_{cat}/K_m) = {}^{1}(k_{cat}/K_m) + {}^{2}(k_{cat}/K_m) \quad (5)$$

Plots of log k_{cat} or log (k_{cat}/K_m), as a function of the leaving group pK_a, were fit to equations 6 and 7, respectively, where β is the Brønsted coefficient and C is the y-intercept.

$$\log\ k_{cat} = \beta\ pk_a + C \quad (6)$$

$$\log\ (k_{cat}/K_m) = \beta\ pk_a + C \quad (7)$$

Absorbance values for total hydrolysis reactions were converted to fraction hydrolyzed according to eqn. 8, where A is absorbance at any time, A_o is the initial absorbance, and ΔA is the total change in absorbance due to hydrolysis. Data were plotted as fraction hydrolyzed as a function of time and fit to eqn. 9, where a is the magnitude of the exponential phase, t is time in seconds and k is the observed exponential rate constant. Dividing the observed rate constant k by enzyme concentration yields the k_{cat}/K_m for the reaction.

$$F = \frac{A - A_o}{\Delta A} \quad (8)$$

$$F = a\left(1 - e^{-kt}\right) \quad (9)$$

For the minimal kinetic mechanism of the *Sb*-PTE-catalyzed reaction presented in Scheme 2, the values of k_{cat} and k_{cat}/K_m are dependent on the relative values of the microscopic rate constants as depicted in eqns. 10 and 11.[12] The effects of changes in solvent viscosity on the values of k_{cat}/K_m were obtained in the presence of variable amounts of sucrose. The ratio of k_{cat}/K_m in the absence, $(k_{cat}/K_m)_o$, and in the presence of the viscogen, $(k_{cat}/K_m)_\eta$, was plotted as a function of the relative viscosity according to eqn. 12.[11] The profiles for the variation of k_{cat} or k_{cat}/K_m with pH were fit to equation 13, where y is the value of k_{cat} or k_{cat}/K_m and c is the pH-independent value of y.

$$k_{cat} = (k_3 k_5)/(k_3 + k_5) \quad (10)$$

$$k_{\text{cat}}/K_m = (k_1 k_3)/(k_2 + k_3) \quad (11)$$

$$(k_{\text{cat}}/K_m)_o/(k_{\text{cat}}/K_m)\eta = (k_3\eta_{\text{rel}} + k_2)/(k_2 + k_3) \quad (12)$$

$$\log y = \log\left[\frac{c}{1 + 10^{(pK_a - pH)}}\right] \quad (13)$$

Heavy Atom Isotope Effect Measurements.

Kinetic isotope effects (KIEs) on the *Sb*-PTE-catalyzed hydrolysis of paraoxon were measured using the competitive method, and thus are isotope effects on $k_{\text{cat}}/K_{\text{m}}$.[18] Scheme 3 illustrates the three positions where KIEs were measured in the substrate paraoxon (**5**) and the designations used.

Natural abundance paraoxon was used for measurements of $^{15}(k_{\text{cat}}/K_{\text{m}})$. The ^{18}O KIEs, $^{18}(k_{\text{cat}}/K_{\text{m}})_{\text{bridge}}$ and $^{18}(k_{\text{cat}}/K_{\text{m}})_{\text{nonbridge}}$, were measured by the remote label method in which the nitrogen atom in the *p*-nitrophenyl leaving group is used as a reporter for ^{18}O fractionation.[19] The mixtures of isotopic isomers used for each of the ^{18}O KIEs are shown in Scheme 4. The synthesis of each of the isotopic isomers was as previously described.[19] Reactions for the determinations of isotope effects were performed in triplicate. For each reaction ~30 mg of paraoxon was dissolved in 50 mL of CHES, pH 9.0, at 25 °C and 0.5 mL of a 100 mM stock solution of $MnCl_2$ was added. Sufficient enzyme was then added to give from 40% to 60% conversion of the substrate in 2 h.

Reaction progress was monitored periodically by adding an aliquot of the reaction mixture to phosphate buffer at pH 9.0 and measuring the absorbance at 400 nm. When reactions had reached at least 40% completion, unreacted paraoxon was extracted with methylene chloride (3 × 50 mL). The methylene chloride fractions were combined, and after removal of solvent by rotary evaporation, the residual paraoxon was completely hydrolyzed by addition of 50 mL of 0.1 N NaOH and stirring for 12 h. The aqueous layer from the methylene chloride extractions contained the *p*-nitrophenol liberated by the *Sb*-PTE catalyzed reaction. The fraction of reaction of each trial was determined by assaying both aqueous solutions for *p*-nitrophenol at 400 nm in basic solution. The aqueous layer after methylene chloride extraction, containing the enzymatic product *p*-nitrophenol, was titrated to pH <5 and extracted with ether (3 × 50 mL). A similar treatment of the hydrolyzed residual substrate samples was used to isolate the *p*-nitrophenol produced from the residual substrate after partial enzymatic reaction. The *p*-nitrophenol samples were purified by sublimation and analyzed by isotope ratio mass spectrometry to determine the $^{15}N/^{14}N$ ratios of the nitrophenol samples for the product (R_p), and for the residual substrate (R_s). Separately,

samples of the substrate were subjected to total hydrolysis and similarly treated to determine the $^{15}N/^{14}N$ ratio in the original mixed substrate (R_o). Each KIE experiment permits two independent determinations of the isotope effect, one from R_s and the other from R_p, using equations 14 and 15.[20]

$$\text{isotope effect} = \log(1-f)/\log\left[(1-f)\left(R_S/R_O\right)\right] \quad (14)$$

$$\text{isotope effect} = \log(1-f)/\log\left[1-f\left(R_P/R_O\right)\right] \quad (15)$$

For each isotope effect measured, the values calculated from R_o and R_p and from R_o and R_s were averaged to give the results reported in Table 2. The $^{15}(k_{cat}/K_m)$ is given directly from these equations. For the ^{18}O isotope effects, the observed KIEs were corrected for the ^{15}N isotope effect and for incomplete levels of isotopic incorporation (see Supplemental Information). The equations used for these corrections and their derivations have been described.[21]

RESULTS

Optimization of *Sb*-PTE Assay Conditions.

Previous studies of the kinetic characteristics of *Sb*-PTE utilized HEPES or CHES buffer.[2, 9, 10, 15] While attempting to determine the pH-dependence of the reactions catalyzed by *Sb*-PTE it was noted that the enzyme displayed a ~2-fold greater activity when TRIS was used as the buffer, rather than HEPES, at pH 8.5. Subsequent tests demonstrated that this increase in activity appeared to be due to the presence of the primary amine from this buffer, and that the increase in activity could be replicated by the inclusion of NH_4^+ in the assays. It was found that inclusion of 100 mM NH_4Cl resulted in a uniform catalytic activity regardless of the buffer used. Subsequent assays for the pH-rate profile and Brønsted analysis utilized a combination buffer, which could be used over a wide range of pH values and was supplemented with 100 mM NH_4Cl.

pH-Rate Profiles for *Sb*-PTE.

The profiles for the effects of pH on the values of the catalytic constants for the hydrolysis of paraoxon (**5**) and diethyl phenyl phosphate (**17**) by *Sb*-PTE were determined (Figure 2). The dependence of the kinetic parameters, k_{cat} and k_{cat}/K_m, with pH are characterized by a single ionization indicated by a slope of +1 below ~7.0 and a plateau above pH 8.0. A fit of the data to eqn. 13 gives the pK_a values from the log k_{cat} profile of 7.9 ± 0.1 and for the k_{cat}/K_m profile of 7.4 ± 0.1. Fitting the data for diethyl phenyl phosphate gives pK_a values of 7.3 ± 0.1 and 7.1 ± 0.1 for k_{cat} and k_{cat}/K_m, respectively (data not shown).

Multiple Products from Single Substrate.

A series of diethyl (**1**-**18**) and dibutyl (**19**–**27**) phosphotriesters with leaving groups of variable pK_a were tested for the production of alternative products using ^{31}P-NMR

spectroscopy. Multiple products were formed from the hydrolysis of all but two of these compounds by *Sb*-PTE (Table 1). To determine if the product ratios varied with pH, experiments were conducted at pH values ranging from 7–10 with 2.0 mM diethyl phenyl phosphate (**17**), and the product composition analyzed by ^{31}P-NMR spectroscopy. It was found that the product ratios were constant at all of the tested pH values (Figure S1). To determine if the product ratios were valid for the subsequent analysis of k_{cat}/K_m, the product ratios derived from the hydrolysis of diethyl *m*-fluorophenyl phosphate (**14**) were determined using an initial concentration 2.0 mM, 500 μM and 10 μM of this substrate. Reactions with the lowest concentration of substrate were conducted in a higher reaction volume and subsequently concentrated after total hydrolysis by *Sb*-PTE. The products were analyzed by ^{31}P-NMR spectroscopy and it was found that the product ratios did not vary with the initial substrate concentration (Figure S2).

Steric Effects of Phenyl Substitution.

The usefulness of any chemical series for linear free energy analysis requires the ability to alter the pK_a without introducing substantial steric effects. The catalytic activity of *Sb*-PTE was measured for the diethyl phophotriester series (**1–18**), which utilized substituted phenols as the leaving group (Table 1). Paraoxon (**5**) with a *p*-nitrophenol leaving group is a prototypical substrate for phosphotriesterase activity. Adding an additional fluoride substitution in the meta-position (compound **4**) increases activity as expected, but the mono- (compound **2**) or di- (compound **1**) substitution of fluoride in the *ortho*-position results in a loss of activity despite nearly three units lower pK_a. Similarly, the presence of a *p*-carbonyl substituent (compounds **7**, **9**, **11**, and **12**) results in dramatically more ethyl cleavage than other compounds with similar pK_a values. The unsubstituted phenyl (compound **17**) gives a k_{cat}/K_m of 1.5×10^4 $M^{-1}s^{-1}$ and 23% cleavage of the phenyl group. A para-substitution of fluoride (**16**) or chloride (**15**) diminishes the enzymatic efficiency by more than 4-fold and further enhances ethyl cleavage. Substitution of the fluoride at the *meta*-position rather than the *para*- position (compound **14**) results in an order of magnitude increase over the unsubstituted phenol and results in the primary product arising from phenol cleavage. These effects demonstrate that both catalytic activity and product distribution in the reaction catalyzed by *Sb*-PTE is sensitive to steric effects from substitution on the phenyl ring.

The dibutyl series of compounds (**19–27**) showed much smaller steric effects (Table 1). The two compounds that did show apparent steric effects were compounds **20** and **25**. Compound **20**, which contains a carbonyl substitution on the phenyl ring, shows ~5-fold less activity than the unsubstituted phenol. Compound **25** contains a carbonyl substitution on C-2 of one butyl group, which results in nearly no cleavage of the unsubstituted butyl groups for this compound.

Brønsted Analysis.

The kinetic constants for the enzyme-catalyzed hydrolysis of the diethyl (**1**-**18**) and dibutyl (**19**-**27**) series of compounds were measured (Table 1). Since multiple products were formed from a single substrate in most cases, the kinetic constants for the total hydrolysis ($^{T}k_{cat}$ and $^{T}(k_{cat}/K_m)$), and the two possible pairs of reaction products; ($^{1}k_{cat}$ and $^{1}(k_{cat}/K_m)$ for the phenol or substituted butanol, and $^{2}k_{cat}$ and $^{2}(k_{cat}/K_m)$ for ethanol or butanol) were

calculated from the spectroscopically determined rates of product formation and the product ratios determined by ^{31}P-NMR spectroscopy. The kinetic constants were plotted as a function of the pK_a of the most activated leaving group. For compounds **1**-**18** the plot of log $^{1}k_{cat}$ versus the pK_a of the leaving phenol shows a decrease in activity with an increase in pK_a (Figure 3a). While there is significant scatter in the data there is an overall trend with no upper plateau at the lower pK_a values. A linear fit to the data gives a β-value of −0.3 ± 0.1. The plot of log $^{1}(k_{cat}/K_m)$ versus the pK_a of the leaving group also exhibits a decrease in value as the pK_a increases with an apparent β-value of −0.3 ± 0.1 (Figure 3b). For hydrolysis of the ethyl substituent, there is no obvious dependence of the most activated leaving group pK_a for either $^{2}k_{cat}$ or $^{2}(k_{cat}/K_m)$ (Figures 3c and 3d). The kinetic constants for total substrate hydrolysis exhibit β-values of −0.2 ± 0.1 and −0.2 ± 0.1 for $^{T}k_{cat}$ and $^{T}(k_{cat}/K_m)$, respectively (Figures 3e and 3f).

The trends in activity with the pK_a of the leaving group were much clearer with the series of dibutyl phosphate compounds (**19**-**27**). In this case the leaving group is either a phenol (**19**-**21**) butylthiol (**22**) or a substituted butyl alcohol (**23**-**27**). For these compounds the hydrolysis of the leaving group with the lowest pK_a exhibits a β-value of −0.33 ± 0.04 for $^{1}k_{cat}$ and −0.32 ± 0.05 for $^{1}(k_{cat}/K_m)$ (Figure 4a and 4b). Hydrolysis of the unactivated butanol group shows a similar trend with the pK_a of the most activated group giving a slope of −0.23 ± 0.07 and −0.23 ± 0.08 for $^{2}k_{cat}$ and $^{2}(k_{cat}/K_m)$, respectively (Figures 4c and 4d). The rate constants for total hydrolysis ($^{T}k_{cat}$ and $^{T}k_{cat}/K_m$)) have β-values of −0.31 ± 0.04 and −0.30 ± 0.05, respectively (Figures 4e and 4f).

Solvent Viscosity Effects.

To further probe the catalytic mechanism, the solvent viscosity effects on k_{cat}/K_m were measured with both paraoxon (**5**) and dibutyl phenyl phosphate (**21**). In both cases there is a modest viscosity-independent enhancement of the reaction rate in the presence of sucrose, but the slope of the viscosity plots is negligible for both substrates (−0.017 ± 0.004 for paraoxon (**5**) and −0.010 ± 0.006 for dibutyl phenyl phosphate, **21**) (Figure 5).

Solvent Deuterium Isotope Effects.

The solvent kinetic isotope effects on k_{cat}/K_m were measured with paraoxon (**5**) and diethyl *m*-fluorophenyl phosphate (**14**) at pH 8.5 and 9.0. For paraoxon, the leaving group is expected to be deprotonated at both pH values examined, while for diethyl *m*-fluorophosphate, the leaving group is expected to be largely protonated at pH 8.5 and partially deprotonated at pH 9.0. At pH values of 8.5 and 9.0 the solvent isotope effects for hydrolysis of paraoxon are quite small with values of 0.88 ± 0.03 and 1.05 ± 0.03, respectively. For diethyl *m*-fluorophenyl phosphate, the solvent isotope effects are also quite small with values of 1.15 ± 0.01 at pH 8.5 and 0.90 ± 0.1 at pH 9.0. Thus, there is essentially no effect on k_{cat}/K_m for either substrate when D_2O is substituted for H_2O.

To determine if there is a solvent deuterium effects on k_{cat}, steady state kinetics were measured with paraoxon in H_2O and D_2O at pH 9.0 and determined to be 1.31 ± 0.02. This finding was further verified by examining the product ratios for the reactions catalyzed in either H_2O or D_2O at pH 8.5 using ^{31}P-NMR. No significant changes to the product ratios

were observed for either substrate when the reaction was conducted in D_2O, suggesting that protonation of the leaving group is not rate limiting for either phenyl or alkyl cleavage. The enzymatic results are similar to the alkaline hydrolysis of these compounds where the solvent deuterium isotope effects for paraoxon (**5**) and diethyl *m*-fluorophenyl phosphate (**14**) are 0.95 ± 0.01 and 0.88 ± 0.05, respectively.

Heavy Atom Isotope Effects.

The heavy atom kinetic isotope effects on the *Sb*-PTE catalyzed hydrolysis of paraoxon (**5**) were determined to address the transition state for cleavage of the P-O bond of the substrate. The primary isotope effect $^{18}(k_{cat}/K_m)_{bridge}$ gives a measure of the degree of cleavage of the P-O bond, whereas the secondary isotope effect $^{18}(k_{cat}/K_m)_{nonbridge}$ is defined by changes in bond order and to bending and torsional vibrational modes.[18] The secondary $^{15}(k_{cat}/K_m)$ is a measure of charge development on the nitrophenyl leaving group. The primary and secondary isotope effects for *Sb*-PTE are provided in Table 2 for hydrolysis of paraoxon, along with the previously determined values for the alkaline and *Pd*-PTE catalyzed hydrolysis of paraoxon (**5**) and diethyl p-carbamoylphenyl phosphate (**12**).

DISCUSSION

pH-Rate Profile.

The pH-rate profile for *Sb*-PTE was determined using paraoxon (**5**) as the substrate. For both k_{cat} and k_{cat}/K_m, the pH-rate profiles exhibit a dependence on a single ionization with pK_a values of 7.9 and 7.4, respectively. Diminution in catalytic activity at high pH is not observed for the hydrolysis of paraoxon up to pH 10.5. The loss of activity at the lower pH is consistent with the protonation of the bridging hydroxide that is proposed to be utilized for nucleophilic attack of the substrate.[25] A separate general acid for protonation of the leaving group is unlikely to be needed for the efficient release of *p*-nitrophenolate. However, similar results were obtained for hydrolysis of diethyl phenyl phosphate (**17**), a substrate with a poorer phenolic leaving group. The enzyme must be able to effectively protonate the leaving group for efficient catalysis, but the lack of a loss of activity at high pH is inconsistant with a separate general acid serving this role, unless it occurs after the rate-limiting step. In addition, *Sb*-PTE has been shown to catalyze hydrolysis of the ethyl and butyl esters in many of the compounds utilized in this investigation. Therefore, the enzyme must also be able to effectively protonate these leaving groups since there is no pH dependence on the product ratios determined for these substrates.

Brønsted Analysis.

Previously, we have shown that *Sb*-PTE is able to catalyze the hydrolysis of substrates with relatively unactivated leaving groups with catalytic efficiencies similar to the cleavage of *p*-nitrophenol.[15] The effect of the pK_a of the leaving group on k_{cat} and k_{cat}/K_m was measured with two series of substrates. In the first series a diethyl phosphate core was utilized with a series of substituted phenols and a second series utilized a dibutyl phosphate core with substituted phenols and modified butyl substituents. For the dibutyl phosphate series, the Brønsted β-coefficients for k_{cat} and k_{cat}/K_m were determined to be approximately −0.3 for the net hydrolysis of the substrate. This result is consistent with the development of a

relatively small amount of negative charge in the leaving group during the transition state.[26] For comparison, the β-coefficient for the alkaline hydrolysis of a similar series of substrates is −0.43.[14] The relatively linear Brønsted plot for this series of substrates is also fully consistent with P-O bond cleavage as the rate-limiting step in the reaction.[11, 19, 27] Interestingly, when the rate of hydrolysis for the un-activated ester is plotted as a function of the pK_a of the more activated group, a linear relationship is observed with a β-value of −0.23 suggesting that in the transition state there is a dispersal of charge to the unreactive ester groups as well as to the leaving group.

With the diethyl phosphate series of substrates there is considerable scatter in the data, likely due to steric constraints in the enzymatic system by the substituted phenols (Figure 3). Interpretation of these results is more complicated because of the differential rate constants for substrates having leaving groups of nearly identical pK_a values (*e.g.* compounds **8** and **9**) and significant disparities in the relative magnitude of ethyl versus phenyl hydrolysis (*e.g.* compounds **14** and **15**). In any event, *Sb*-PTE can catalyze the hydrolysis of the ethyl substituent with relatively high efficiency even in substrates with significantly better leaving groups. This fact is exemplified with diethyl phenyl phosphate (**17**) hydrolysis where the ethyl substituent is hydrolyzed nearly four-fold more often than the phenyl substituent.

The Brønsted analysis also suggests that P-O bond cleavage is rate limiting for k_{cat} and k_{cat}/K_m for the dibutyl series of substrates tested for this investigation. The effects of changes in solvent viscosity on k_{cat}/K_m support this conclusion. When sucrose was used to increase the relative viscosity from 1.1 to 2.5, there was essentially no effect on the relative magnitude of k_{cat}/K_m. Thus, for both paraoxon (**5**) and dibutyl phenyl phosphate (**21**) the rate constant for the dissociation of substrate from the Michaelis complex (k_2) is significantly bigger than the first-order rate constant for the conversion of substrate to products (k_3). Therefore, the substrates for *Sb*-PTE are not “sticky” and the net rate for substrate turnover is dictated by the relative magnitude of k_3.

Kinetic Isotope Effects with Paraoxon.

The kinetic isotope effects (KIEs) report on the transition state for cleavage of the P-O ester bond in the substrate. Two of the three KIEs report on the leaving group, while the third reports on the structure of the phosphorus center in the transition state. The secondary isotope effect $^{15}(k_{cat}/K_m)$ measures negative charge delocalized into the nitro group due to contributions from a quinonoid resonance form of the *p*-nitrophenolate anion involving the nitrogen atom.[18] As a result, the ^{15}K equilibrium isotope effect (EIE) for deprotonation of *p*-nitrophenol is normal.[28] In enzymes catalyzing phosphoryl transfer of substrates with this leaving group, this isotope effect has a maximum of 1.0030 in enzymes lacking general acid catalysis and a late transition state with extensive P-O bond fission. An earlier transition state, or charge neutralization by general acid catalysis, reduces the magnitude.[18]

The primary isotope effect $^{18}(k_{cat}/K_m)_{bridge}$ provides a measure of the degree of cleavage of the P-O bond in the transition state. This KIE reaches a maximum value of ~1.03 in a late transition state with nearly full bond fission.[18] This isotope effect has a normal contribution from P-O bond fission, but protonation or metal ion coordination will result in a diminished effect.[29] For this reason, the magnitude of $^{18}(k_{cat}/K_m)_{bridge}$ in phosphatase-catalyzed

reactions is reduced in enzymes with functional general acid catalysis compared to their general acid mutants. General acid catalysis reduces $^{18}(k_{cat}/K_m)_{bridge}$ to ~1.015 in protein tyrosine phosphatases, and metal ion complexation reduces it to 1.009 in an alkaline phosphatase mutant (R166S) for which chemistry is rate-limiting.[18, 29]

The secondary isotope effect $^{18}(k_{cat}/K_m)_{nonbridge}$ is affected by changes in bond order and changes to bending and torsional vibrational modes.[18] If the transition state is associative, resembling a phosphorane, the *pi* bond to the nonbridging oxygen atom is lost and the phosphorus atom becomes more trigonal bipyramidal. The loss of bond order will result in a normal effect, while the effect from changes to bending modes should be inverse. The latter effects can be dominant for secondary isotope effects on an atom bonded to a center undergoing hybridization changes. For example, α-secondary deuterium isotope effects are normal for hybridization changes of the type sp^3 to sp^2 or sp^2 to sp.[18] The bond order changes at the nonbridge oxygen atom lead one to expect $^{18}k_{nonbridge}$ to be normal for an associative transition state, but negligible in a more symmetric S_N2-like process. Coordination to a metal center can both increase or decrease the observed $^{18}k_{nonbridge}$ isotope effects.[29]

Phosphate triesters are thought to have more associative transition states than monoesters, and trends in KIE data from uncatalyzed hydrolysis reactions of phosphate esters suggest that bond order changes are the dominant contributors.[29, 30] The measured $^{18}k_{nonbridge}$ effects are inverse (though very small) for the loose transition states of monoester reactions, but are normal for diester and triesters.[18] In the more associative transition states of triester reactions, bond fission to the leaving group is less advanced than in monoester reactions.[30, 31] This is reflected in the smaller ^{15}N isotope effect in the alkaline hydrolysis of paraoxon, relative to uncatalyzed reactions of the monoester *p*-nitrophenyl phosphate, in which this isotope effect is about 4-fold larger.[24] The same trend is seen in the comparative ^{18}O bridge effects in reactions of the two esters.[30, 31]

The interpretation of isotope effects on enzymatic reactions must be concerned with the question of to what degree the chemical step is rate-determining, and whether the full isotope effects on the transition state are observed. Commitments to catalysis or rate-limitation by non-chemical steps will suppress all isotope effects in the same ratio. In the case of *Sb*-PTE the lack of solvent viscosity effects rules out a commitment to catalysis, while the linear Brønsted plots are consistent with chemistry as being rate limiting for the reaction with paraoxon. The lack of a solvent deuterium isotope effects suggests that the KIEs are not masked by protonation of the leaving group. Additionally, KIEs for the corresponding uncatalyzed reaction are usually taken as a benchmark for comparison. In this particular reaction, the KIEs measured for the *Sb*-PTE catalyzed cleavage of paraoxon (**5**) were found to be comparable to those of the alkaline hydrolysis (Table 2). This further indicates the chemical step is rate-limiting, despite the lability of the leaving group. Catalysis by *Sb*-PTE requires two divalent metal ions, which could either serve to activate a nucleophilic water molecule or coordinate the leaving group. Examples of both kinds of interaction have precedent in enzymes that catalyze phosphoryl transfer.[25, 29] However, the KIE data are more consistent with the metal ion serving the role of activating the nucleophile, as previously proposed.[9]

The leaving group isotope effect $^{15}(k_{cat}/K_m)$ for *Sb*-PTE is comparable to the value obtained for alkaline hydrolysis of paraoxon. This means that the leaving group has the same negative charge delocalization in the transition states of both reactions. The somewhat larger primary $^{18}(k_{cat}/K_m)_{bridge}$ effect in the *Sb*-PTE reaction indicates P-O bond fission is at least as advanced, and perhaps more so, compared to alkaline hydrolysis. However, the magnitudes of $^{18}(k_{cat}/K_m)_{bridge}$ and $^{15}(k_{cat}/K_m)$ are each about one-third of their maximal values seen in monoester reactions with this leaving group.[18] This is consistent with the proposal that phosphotriesters have transition states that are less dissociative (less bond fission to the leaving group) than monoesters.[30] *Sb*-PTE catalyzes the hydrolysis of triesters with a wide range of leaving groups, and it is possible that, as in the uncatalyzed reaction with poorer leaving groups, substrates may undergo reactions by even more associative transition states and possibly via a phosphorane intermediate. A highly associative reaction is expected to reveal itself by a normal value for $^{18}(k_{cat}/K_m)_{nonbridge}$. This isotope effect in the *Sb*-PTE catalyzed hydrolysis of paraoxon (**5**) is less than a tenth of the magnitude of nonbridging ^{18}O KIEs in the hydrolysis of triesters with poor leaving groups, which exhibit highly associative transition states. However, tight coordination to a metal center can introduce a negative component to the $^{18}(k_{cat}/K_m)_{nonbridge}$ effect.[29] The $^{18}(k_{cat}/K_m)_{nonbridge}$ effect reported here is not significantly different from that in the alkaline hydrolysis of paraoxon. The overall conclusion from the isotope effects is that chemistry is rate-limiting for the reaction with an early transition state and charge delocalization very similar to what is observed for alkaline hydrolysis.

Further supporting the formation of an early associative transition state is the finding that there is effectively no solvent deuterium isotope effect on either k_{cat} or k_{cat}/K_m. Effective hydrolysis of an unactivated ethyl or butyl ester is expected to require protonation of the leaving group. *Sb*-PTE does not display a solvent isotope effect on k_{cat}/K_m with either "good" (*p*-nitrophenyl) leaving groups where protonation is not required or with "poorer" (phenyl and ethyl) leaving groups where protonation would be more likely. The further finding that there is no effect on the product ratios when the hydrolysis reaction is conducted in D_2O confirms that protonation of the leaving groups is not rate limiting. This is in good agreement with an early associative transition state with subsequent proton transfers being fast.

The Mechanism of the *Sb*-PTE Catalyzed Reaction.

The structure of the binuclear metal center in *Sb*-PTE is presented in Figure 1.[9] The two manganese ions in the active site coordinate a bridging hydroxide or water molecule, which is further hydrogen bonded to the side chain of Glu407. Unfortunately, the three-dimensional structure of *Sb*-PTE has not been determined in the presence of a substrate or bound inhibitor. Since the structure of the binuclear metal center in *Sb*-PTE is remarkably similar to that determined previously for the metal center in *Pd*-PTE, it is assumed that the binding of substrates will be comparable.[14, 32] We therefore postulate that one of the two divalent metal ions (M_β) will function primarily to polarize the phosphoryl oxygen bond of the substrate and that the other divalent cation (M_α) will serve to decrease the pK_a of the bridging water/hydroxide with the assistance of Glu407.[33] It has been shown previously that the reaction catalyzed by *Sb*-PTE proceeds via the direct attack of hydroxide on the

phosphorus center leading to an overall inversion in stereochemistry for the product, in a process that does not involve a covalent reaction intermediate.[10]

Sb-PTE is capable of hydrolyzing a wide range of organophosphate triester substrates. The absence of a solvent viscosity effect and the magnitude of the ^{18}O-isotope effects are consistent with nucleophilic attack of hydroxide as the rate-limiting step during the hydrolysis of substrates by this enzyme. This conclusion is further supported by the systematic decreases in k_{cat} and k_{cat}/K_m when the pK_a of the leaving group is progressively increased from 4–16. The Brønsted-coefficient and the relative size of the ^{18}O-isotope effects for the bridge and nonbridge positions suggest that the transition state for ester hydrolysis is relatively early and is associative. The finding of a single group which must be deprotonated for catalysis makes it is highly likely that the nucleophile for substrate hydrolysis originates from the hydroxide that bridges the two divalent cations in the active site of this enzyme (Figure 1). The structure of *Sb*-PTE was solved with both metal ions in an octahedral geometry with three waters bound to the metal center in addition to the bridging hydroxyl (Figure 6A). It remains possible that one of the terminal water molecules could act as the nucleophile, however the current structural data suggest that both of the waters bound to the β-metal must be displaced to allow substrate binding, leaving only the terminal water on the α-metal.[9] A similar arrangement was observed in a close homolog of *Pd*-PTE, OPDA, where a terminal water/hydroxide was proposed to be the attacking nucleophile.[34] However, it was subsequently found that the pK_a of the terminal water was ~10.[35] Our finding of a catalytic pK_a of 7.4 is more consistent with the nucleophile being the bridging hydroxide, which in the manganese containing *Pd*-PTE has a pK_a of 7.3.[25]

We propose that substrates bind to the active site via the displacement of two water molecules (Wat3 and Wat4) from M_β with the phosphoryl oxygen coordinating to the Mn^{+2} in the place of Wat4 and one of the ester oxygens coordinating to the metal in place of Wat3 (Figure 6B). This positions the central phosphorus core adjacent to the bound hydroxide and further enables the phosphoryl oxygen bond to be effectively polarized by M_β. In this binding orientation the angle between the hydroxyl and the leaving group oxygen is ~180°, and the free oxygen of Glu407 is within hydrogen bonding distance to both the bridging hydroxide and the leaving group oxygen. For substrates with poor leaving groups, we further postulate that Glu407 ultimately functions as a general acid catalyst for protonation of the product since no other residues in the active site can functionally fulfill this role. A similar role as a general acid has been observed for a metal coordinating carboxylate in dihydroorotase, where an aspartate residue transfers a proton from the nucleophile to the leaving group during the reaction.[36]

The proposed catalytic mechanism for *Sb*-PTE is shown in Scheme 5. The phosphoryl oxygen and one of the ester oxygens bind in a bidentate manner to the β-metal allowing polarization of the phosphorus center. The bridging hydroxide attacks the phosphorus center forming a phosphorane-like transition state with delocalization of charge supported by coordination to the metal as well as the electronegative ester groups. Once the phosphorane species is formed, the pK_a of the attacking OH group will be drastically reduced and the proton can be passed to Glu407. In the substrate docked structure of *Sb*-PTE, the free oxygen of Glu407 is 4.0 Å from the leaving group oxygen, which would enable transfer of

the proton to the leaving group, facilitating the collapse of the phosphorane intermediate into products. This mechanism is consistent with the early associative transition state indicated by the relatively small β-values and heavy atom isotope effects. It would appear that formation of the phosphorane-like transition state is the rate limiting step for *Sb*-PTE and subsequent proton transfers are more rapid, accounting for the lack of solvent deuterium effects on the reaction.

Given the lack of a three-dimensional structure with substrate or product bound, it remains possible to propose an alternate reaction mechanism where the leaving group is coordinated to a metal. Such a mechanism would be consistent with the low β-values and heavy atom isotope effects.[18, 29] However, given the apparent identity of the attacking nucleophile as the bridging hydroxide, the current structural data suggest that there is no obvious binding mode which would facilitate proper alignment for nucleophilic attack with the leaving group coordinated to a metal ion without substantial steric clashes with the protein structure.

The Formation of Alternative Products by *Sb*-PTE.

Sb-PTE has the unusual ability to hydrolyze different substituents within the same substrate. For some substrates, such as diethyl pentafluorophenyl phosphate (**3**), the product distribution is dominated by the hydrolysis of the substituted phenol. Whereas in other substrates, such as diethyl *p*-chlorophenyl phosphate (**15**), the product distribution is almost completely derived by the hydrolysis of the ethyl ester. There is a small, but consistent trend of an increase in the fraction of ethyl ester hydrolysis as the pK_a of the substituted phenol increases. For base-catalyzed hydrolysis of organophosphates, the ester bond bearing the leaving group with the lowest pK_a will always be hydrolyzed in preference to the other two possibilities.[30]

Unfortunately, at this time it is not possible to fully explain the remarkable ability of *Sb*-PTE to hydrolyze activated and unactivated esters within the same substrate at comparable rates. The catalytic mechanism in Scheme 5 is proposed to account for all of the experimental evidence currently available and potentially provides an explanation as to how *Sb*-PTE is able to efficiently catalyze the hydrolysis of simple alkyl esters at rates similar to highly activated leaving groups. It is obvious from the data with both the diethyl phosphotriester series and previously reported activity with chiral substrates that steric effects involving both leaving group substitutions as well as the non-reactive ester group play large roles in dictating the product profile of *Sb*-PTE.[15] Although a substrate-bound structure of *Sb*-PTE is not currently available it is likely that at least a portion of the product distribution profile must be dictated by the relative binding affinities of the ester substituents within the confines of the active site. Thus, one can readily imagine that each substrate could bind in any of three possible orientations relative to the attacking nucleophile. The product ratios would then be governed by the inherent chemical propensity for a given ester to be hydrolyzed and the fraction of binding in that orientation.

Comparison to Other Phosphotriesterase Enzymes.

Sb-PTE is the only phosphotriesterase enzyme known to hydrolyze organophosphorus flame retardants. This property of *Sb*-PTE derives from the ability to cleave unactivated leaving

groups. For other phosphotriesterase enzymes the catalytic activity is strongly dependent on the pK_a of the leaving group making the cleavage of unactivated groups impossible. The two-best studied phosphotriesterase enzymes are PON1 and *Pd*-PTE. The Brønsted analyses for both enzymes revealed β-values in excess of −2 indicating very late transition states with near complete bond cleavage.[13, 14] PON1 uses a single catalytic Ca^{2+} metal to polarize the phosphorus center via coordination of the phosphoryl oxygen and the reaction mechanism is somewhat ambiguous, making comparison to *Sb*-PTE difficult.[37]

The metal centers found in *Sb*-PTE and *Pd*-PTE are nearly identical, but the orientation of the substrate binding pocket is substantially different.[9, 32] The native metal in *Sb*-PTE is manganese, which was found in an octahedral geometry for both the α- and β-metals in the three-dimensional crystal structure.[9] In *Pd*-PTE the substrate interacts with the zinc metal center via a single coordination of the phosphoryl oxygen to the β-metal, which is found in a trigonal bipyramidal geometry.[32] This same geometry was found in the structure of manganese substituted *Pd*-PTE as well.[38] A crystal structure of a *Pd*-PTE variant with cobalt as the active site metal was solved with octahedral geometry at both the α- and β-metal sites with two waters bound to the β-site, but a structure with product bound demonstrated a displacement of a single water to allow coordination of the phosphoryl oxygen, while the second water remained bound to the metal.[39]

While there is no substrate- or product-bound structure of *Sb*-PTE, docking a substrate in the active site with the coordination of the phosphoryl oxygen to the β-metal requires the displacement of both waters bound to the β-metal and brings an ester oxygen into place to coordinate to the metal as well.[9] Because of the different orientation of the substrate binding sites to the metal center, this binding conformation is not possible in *Pd*-PTE, and in *Pd*-PTE the carboxylate that hydrogen bonds to the bridging hydroxyl is not positioned to be able to protonate the leaving group.[32]

The transition state of *Pd*-PTE appears to be quite different from that of *Sb*-PTE. Chemistry is not rate-limiting for the hydrolysis of paraoxon with *Pd*-PTE (**5**), and consequently the kinetic isotope effects are quite small (Table 2).[11, 19] The ^{18}O isotope effects with diethyl *p*-carbamoylphenyl phosphate (**12**) are substantially larger where chemistry is rate-limiting, indicating near complete P-O bond cleavage in the transition state (Table 2).[19] The $^{18}O_{nonbridge}$ effect was similarly large (1.0181) indicating an associative pentacoordinate transition state. The ^{18}O isotope effects and β-values observed for *Pd*-PTE indicate a very late pentacoordinate transition state with nearly completed P-O bond cleavage. The transition state for *Sb*-PTE is very early, and subsequent steps including proton transfer are fast. It is quite likely that the alternate binding to the metal center in *Sb*-PTE and the positioning of Glu-407 to protonate the leaving group gives rise to the unique ability of *Sb*-PTE to hydrolyze unactivated leaving groups.

Supplementary Material

Refer to Web version on PubMed Central for supplementary material.

Funding

This work was supported by a grant from the National Institutes of Health (GM 116894). CWB was supported by a USU College of Science summer minigrant.

REFERENCES

[1]. Abe K, Yoshida S, Suzuki Y, Mori J, Doi Y, Takahashi S, and Kera Y (2014) Haloalkylphosphorus hydrolases purified from Sphingomonas sp. strain TDK1 and Sphingobium sp. strain TCM1, Appl. Environ. Microbiol 80, 5866–5873. [PubMed: 25038092]

[2]. Xiang DF, Bigley AN, Ren Z, Xue H, Hull KG, Romo D, and Raushel FM (2015) Interrogation of the Substrate Profile and Catalytic Properties of the Phosphotriesterase from Sphingobium sp. Strain TCM1: An Enzyme Capable of Hydrolyzing Organophosphate Flame Retardants and Plasticizers, Biochemistry 54, 7539–7549. [PubMed: 26629649]

[3]. Maxwell DM, Brecht KM, Koplovitz I, and Sweeney RE (2006) Acetylcholinesterase inhibition: does it explain the toxicity of organophosphorus compounds?, Arch. Toxicol 80, 756–760. [PubMed: 16770629]

[4]. van der Veen I, and de Boer J (2012) Phosphorus flame retardants: properties, production, environmental occurrence, toxicity and analysis, Chemosphere 88, 1119–1153. [PubMed: 22537891]

[5]. Dishaw LV, Powers CM, Ryde IT, Roberts SC, Seidler FJ, Slotkin TA, and Stapleton HM (2011) Is the PentaBDE replacement, tris (1,3-dichloro-2-propyl) phosphate (TDCPP), a developmental neurotoxicant? Studies in PC12 cells, Toxicol. Appl. Pharmacol 256, 281–289. [PubMed: 21255595]

[6]. Isales GM, Hipszer RA, Raftery TD, Chen A, Stapleton HM, and Volz DC (2015) Triphenyl phosphate-induced developmental toxicity in zebrafish: potential role of the retinoic acid receptor, Aquat. Toxicol 161, 221–230. [PubMed: 25725299]

[7]. World Health Organization (1998) Environmental Health Criteria 209, Flame Retardants: Tris(chloropropyl) Phosphate and Tris(2-chloroethyl) Phosphate, World Health Organization, Geneva, Switzerland.

[8]. Reemtsma T, Quintana JB, Rodil R, Garcia-Lopez M, and Rodriguez I (2008) Organophosphorus flame retardants and plasticizers in water and air I. Occurrence and fate, Trends Analyt. Chem 27, 727–737.

[9]. Mabanglo MF, Xiang DF, Bigley AN, and Raushel FM (2016) Structure of a Novel Phosphotriesterase from Sphingobium sp. TCM1: A Familiar Binuclear Metal Center Embedded in a Seven-Bladed beta-Propeller Protein Fold, Biochemistry 55, 3963–3974. [PubMed: 27353520]

[10]. Bigley AN, Xiang DF, Ren Z, Xue H, Hull KG, Romo D, and Raushel FM (2016) Chemical Mechanism of the Phosphotriesterase from Sphingobium sp. Strain TCM1, an Enzyme Capable of Hydrolyzing Organophosphate Flame Retardants, J. Am. Chem. Soc 138, 2921–2924. [PubMed: 26907457]

[11]. Caldwell SR, Newcomb JR, Schlecht KA, and Raushel FM (1991) Limits of diffusion in the hydrolysis of substrates by the phosphotriesterase from Pseudomonas diminuta, Biochemistry 30, 7438–7444. [PubMed: 1649628]

[12]. Donarski WJ, Dumas DP, Heitmeyer DP, Lewis VE, and Raushel FM (1989) Structure-activity relationships in the hydrolysis of substrates by the phosphotriesterase from Pseudomonas diminuta, Biochemistry 28, 4650–4655. [PubMed: 2548585]

[13]. Khersonsky O, and Tawfik DS (2005) Structure-reactivity studies of serum paraoxonase PON1 suggest that its native activity is lactonase, Biochemistry 44, 6371–6382. [PubMed: 15835926]

[14]. Hong SB, and Raushel FM (1996) Metal-substrate interactions facilitate the catalytic activity of the bacterial phosphotriesterase, Biochemistry 35, 10904–10912. [PubMed: 8718883]

[15]. Bigley AN, Narindoshvili T, Xiang DF, and Raushel FM (2018) Multiple Reaction Products from the Hydrolysis of Chiral and Prochiral Organophosphate Substrates by the Phosphotriesterase from Sphingobium sp. TCM1, Biochemistry 57, 1842–1846. [PubMed: 29513982]

[16]. Chapman E, and Wong CH (2002) A pH sensitive colorometric assay for the high-throughput screening of enzyme inhibitors and substrates: a case study using kinases, Bioorg. Med. Chem 10, 551–555. [PubMed: 11814841]

[17]. Salomaa P, Schaleger LL, and Long FA (1964) Solvent Deuterium Isotope Effects on Acid-Base Equilibria, J. Am. Chem. Soc 86, 1–7.

[18]. Hengge AC (2002) Isotope effects in the study of phosphoryl and sulfuryl transfer reactions, Acc. Chem. Res 35, 105–112. [PubMed: 11851388]

[19]. Caldwell SR, Raushel FM, Weiss PM, and Cleland WW (1991) Transition-state structures for enzymatic and alkaline phosphotriester hydrolysis, Biochemistry 30, 7444–7450. [PubMed: 1649629]

[20]. Bigeleisen J, and Wolfsberg M (1958) Theoretical and Experimental Aspects of Isotope Effects in Chemical Kinetics, Adv. Chem. Phys 1, 15–76.

[21]. Cleland WW (2006) Enzyme Mechanisms from Isotope Effects, In Isotope Effects in Chemistry and Biology (Kohen A, and Limbach H-H, Ed.), pp 915–930, CRC Press, Boca Raton.

[22]. Gasbarri C, and Angelini G (2014) Spectroscopic investigation of fluorinated phenols as pH-sensitive probes in mixed liposomal systems, Rsc Adv 4, 17840–17845.

[23]. International Union on Pure and Applied Chemsitry. Commission on Equilibrium Data (1979) In Ionisation constants of organic acids in aqueous solution (Serjeant EP. a,D. B, Ed.), Pergamon Press, Oxford.

[24]. Hengge AC, and Cleland WW (1990) Direct Measurement of Transition-State Bond-Cleavage in Hydrolysis of Phosphate-Esters of P-Nitrophenol, J. Am. Chem. Soc 112, 7421–7422.

[25]. Samples CR, Howard T, Raushel FM, and DeRose VJ (2005) Protonation of the binuclear metal center within the active site of phosphotriesterase, Biochemistry 44, 11005–11013. [PubMed: 16101284]

[26]. Fersht A (1999) Structure and mechanism in protein science: a guide to enzyme catalysis and protein folding, W. H. Freeman and Company, New York.

[27]. Jencks WP, and Gilchrist M (1968) Nonlinear Structure-Reactivity Correlations Reactivity of Nucleophilic Reagents toward Esters, J. Am. Chem. Soc 90, 2622–2637.

[28]. Hengge AC, and Cleland WW (1990) Direct measurement of transition-state bond cleavage in hydrolysis of phosphate esters of p-nitrophenol, J. Am. Chem. Soc 112, 7421–7422.

[29]. Zalatan JG, Catrina I, Mitchell R, Grzyska PK, O'Brien PJ, Herschlag D, and Hengge AC (2007) Kinetic isotope effects for alkaline phosphatase reactions: Implications for the role of active-site metal ions in catalysis, J. Am. Chem. Soc 129, 9789–9798. [PubMed: 17630738]

[30]. Anderson MA, Shim H, Raushel FM, and Cleland WW (2001) Hydrolysis of phosphotriesters: Determination of transition states in parallel reactions by heavy-atom isotope effects, J. Am. Chem. Soc 123, 9246–9253. [PubMed: 11562204]

[31]. Hengge AC, Edens WA, and Elsing H (1994) Transition-State Structures for Phosphoryl-Transfer Reactions of P-Nitrophenyl Phosphate, J. Am. Chem. Soc 116, 5045–5049.

[32]. Vanhooke JL, Benning MM, Raushel FM, and Holden HM (1996) Three-Dimensional Structure of the Zinc-Containing Phosphotriesterase with the Bound Substrate Analog Diethyl 4-Methylbenzylphosphonate, Biochemistry 35, 6020–6025. [PubMed: 8634243]

[33]. Aubert SD, Li Y, and Raushel FM (2004) Mechanism for the hydrolysis of organophosphates by the bacterial phosphotriesterase, Biochemistry 43, 5707–5715. [PubMed: 15134445]

[34]. Jackson C, Kim HK, Carr PD, Liu JW, and Ollis DL (2005) The structure of an enzyme-product complex reveals the critical role of a terminal hydroxide nucleophile in the bacterial phosphotriesterase mechanism, Biochim. Biophys. Acta 1752, 56–64. [PubMed: 16054447]

[35]. Ely F, Hadler KS, Gahan LR, Guddat LW, Ollis DL, and Schenk G (2010) The organophosphate-degrading enzyme from Agrobacterium radiobacter displays mechanistic flexibility for catalysis, Biochem. J 432, 565–573. [PubMed: 20868365]

[36]. Thoden JB, Phillips GN Jr., Neal TM, Raushel FM, and Holden HM (2001) Molecular structure of dihydroorotase: a paradigm for catalysis through the use of a binuclear metal center, Biochemistry 40, 6989–6997. [PubMed: 11401542]

[37]. Harel M, Aharoni A, Gaidukov L, Brumshtein B, Khersonsky O, Meged R, Dvir H, Ravelli RB, McCarthy A, Toker L, Silman I, Sussman JL, and Tawfik DS (2004) Structure and evolution of

the serum paraoxonase family of detoxifying and anti-atherosclerotic enzymes, Nat. Struct. Mol. Biol 11, 412–419. [PubMed: 15098021]

[38]. Benning MM, Shim H, Raushel FM, and Holden HM (2001) High resolution X-ray structures of different metal-substituted forms of phosphotriesterase from Pseudomonas diminuta, Biochemistry 40, 2712–2722. [PubMed: 11258882]

[39]. Tsai PC, Fox N, Bigley AN, Harvey SP, Barondeau DP, and Raushel FM (2012) Enzymes for the homeland defense: optimizing phosphotriesterase for the hydrolysis of organophosphate nerve agents, Biochemistry 51, 6463–6475. [PubMed: 22809162]

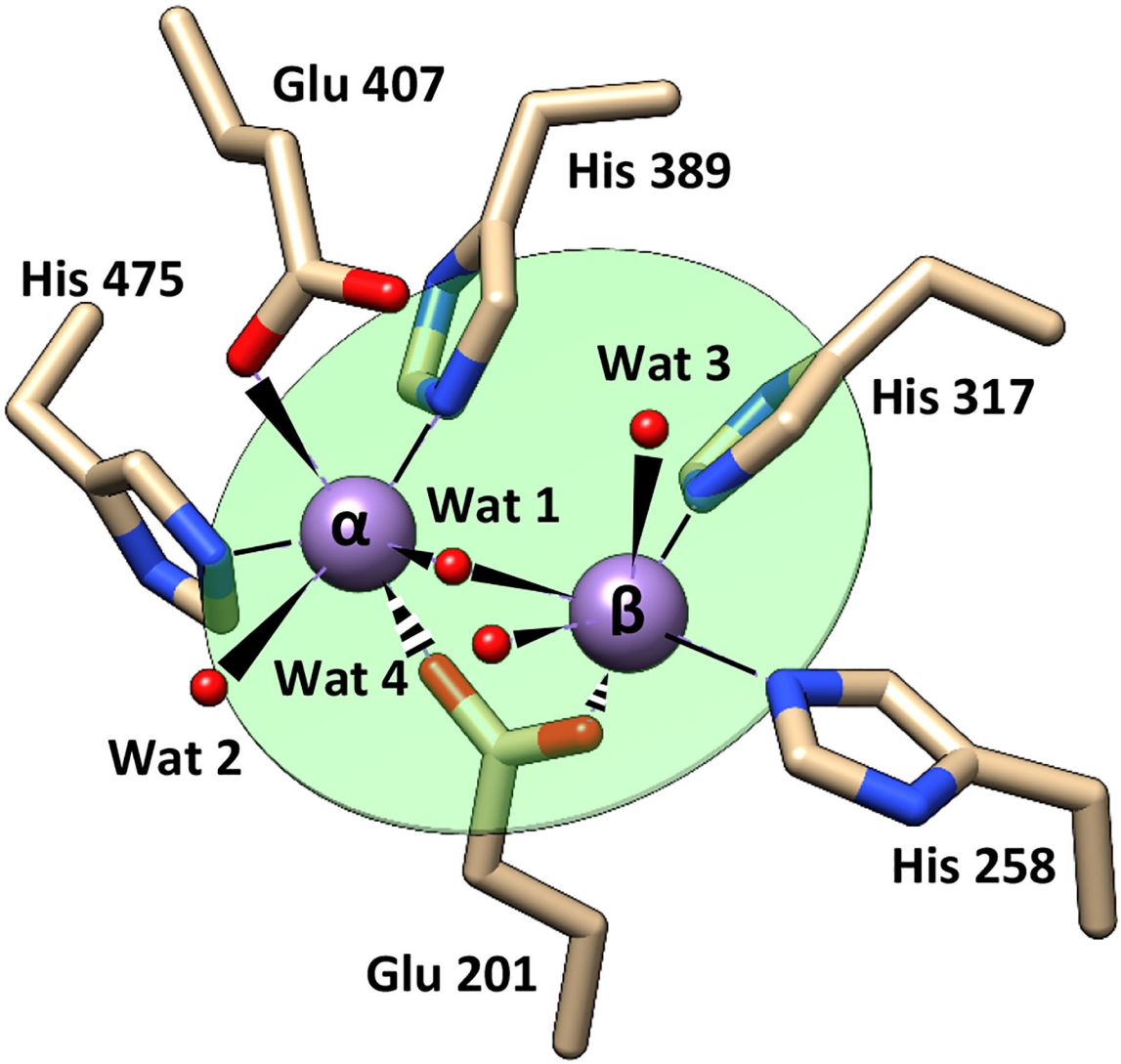

Figure 1.

Binuclear metal center of *Sb*-PTE. The plane of the metal center is defined by the coordinating nitrogen atoms from four histidine residues (green oval). The α-metal is coordinated by Glu201, His389, Glu407, His475, the bridging hydroxide (Wat 1) and an additional water ligand (Wat 2). The β-metal is coordinated by Glu201, His258, His317, the bridging hydroxide (Wat 1) and two additional waters (Wat 3 and Wat 4) from solvent.

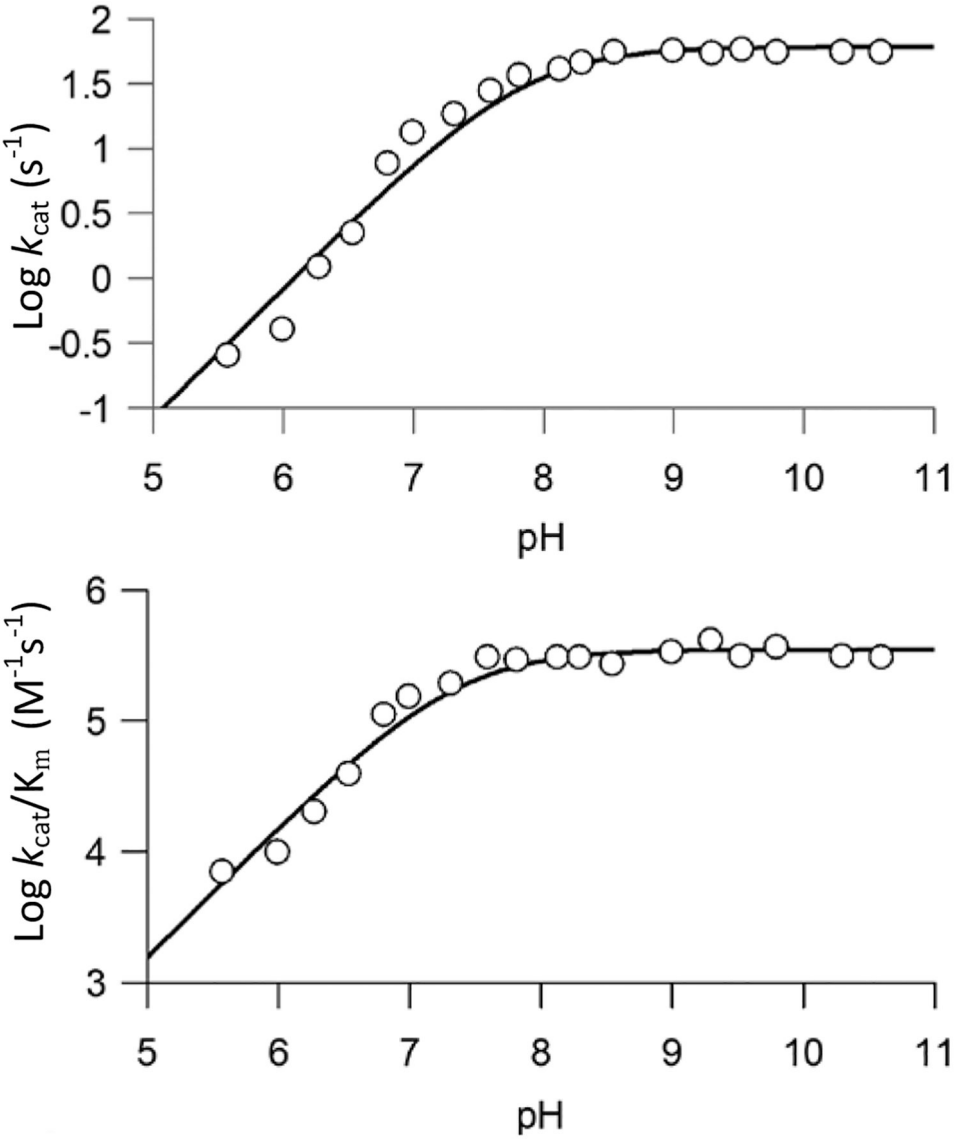

Figure 2:

pH-rate profile for the hydrolysis of paraoxon (**5**) by *Sb*-PTE at 30 °C. The data were fit to eqn. 13. Additional information is provided in the text.

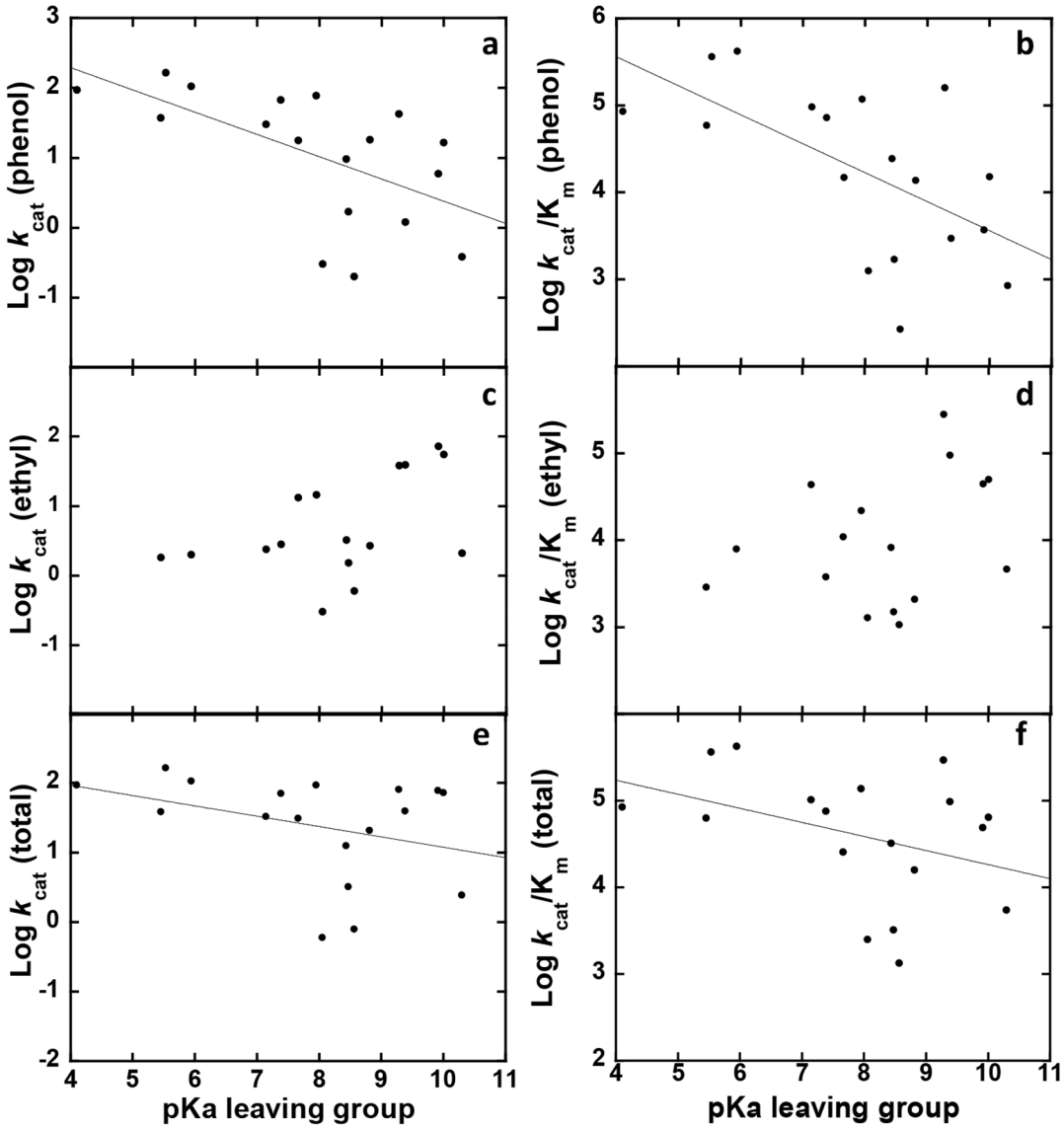

Figure 3.

Brønsted plots for diethyl phosphotriester series compounds **1–18**. Lines are best fit to eqns. 6 or 7 giving β-values of −0.3 for both k_{cat} (R^2 = 0.35) and k_{cat}/K_m (R^2 = 0.37) for phenol leaving group hydrolysis (panels a and b) there is no trend apparent for ethyl cleavage (panels c and d) and a β-value −0.2 for total hydrolysis for both k_{cat} (R^2 = 0.12) and k_{cat}/K_m (R^2 = 0.14) (panels e and f).

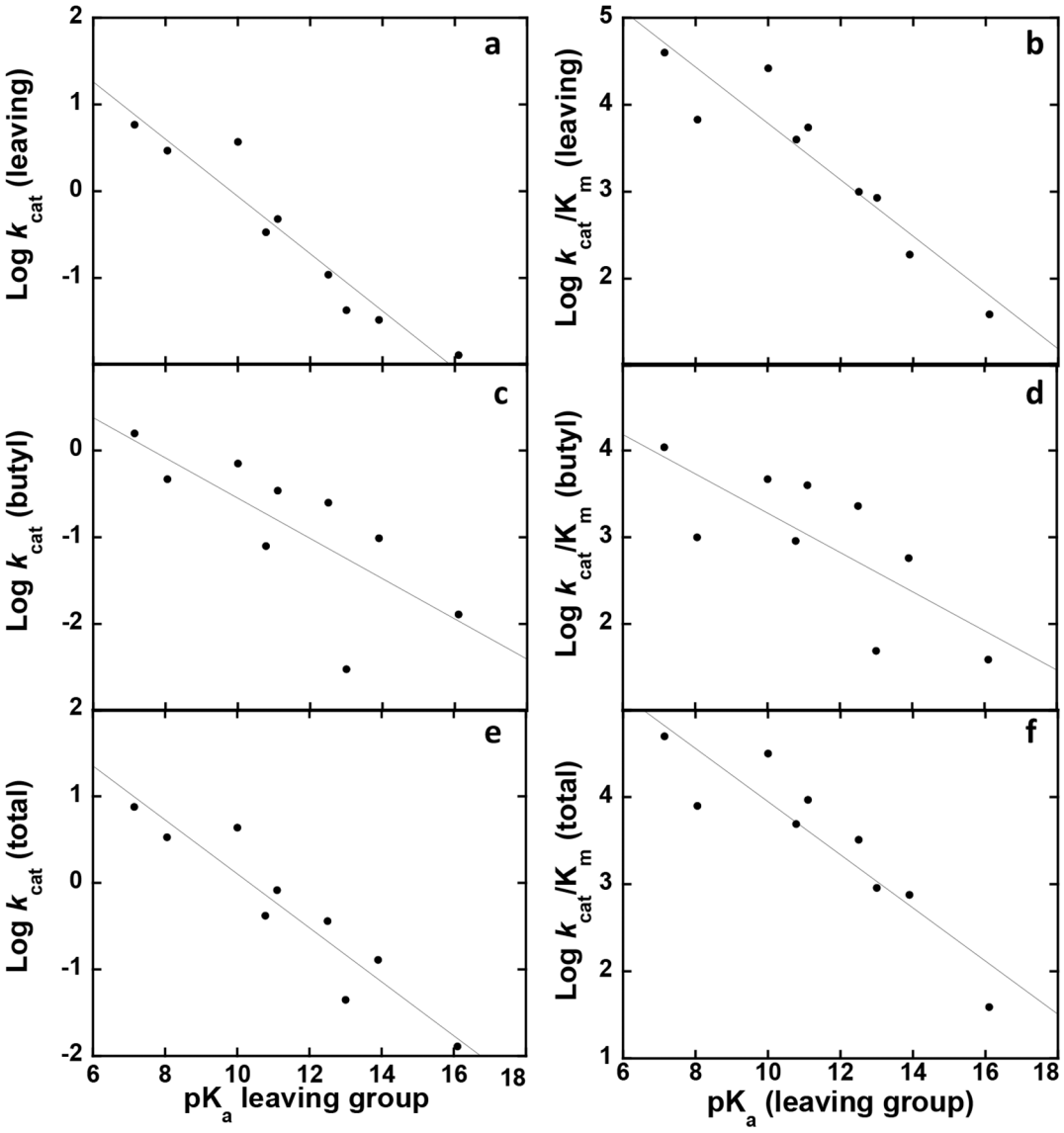

Figure 4.

Brønsted plots for dibutyl phosphotriester series compounds **19–27**. Lines are best fit to equation 6 or 7. β-values are −0.33 (R^2=0.92) and −0.32 (R^2 = 0.87) for k_{cat} and k_{cat}/K_m, respectively, for activated leaving group (panels a and b), −0.23 (R^2 = 0.57) and −0.23 (R^2 = 0.57) for butyl leaving group (panels c and d) and −0.31 (R^2 = 0.87) and −0.30 (R^2 = 0.83) for total hydrolysis rates (panels e and f).

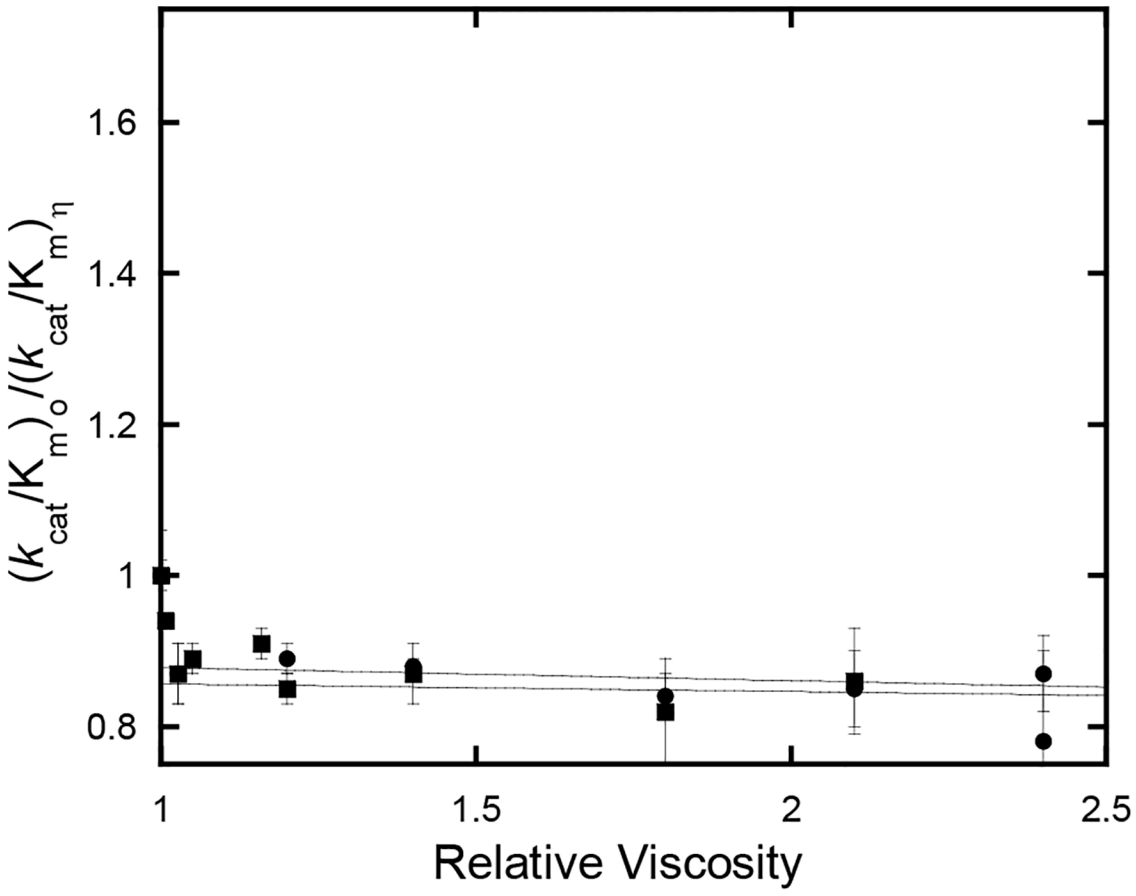

Figure 5.

Solvent viscosity effects of *Sb*-PTE for the hydrolysis of paraoxon (**5**) (●) and dibutyl phenyl phosphate (**21**) (■).

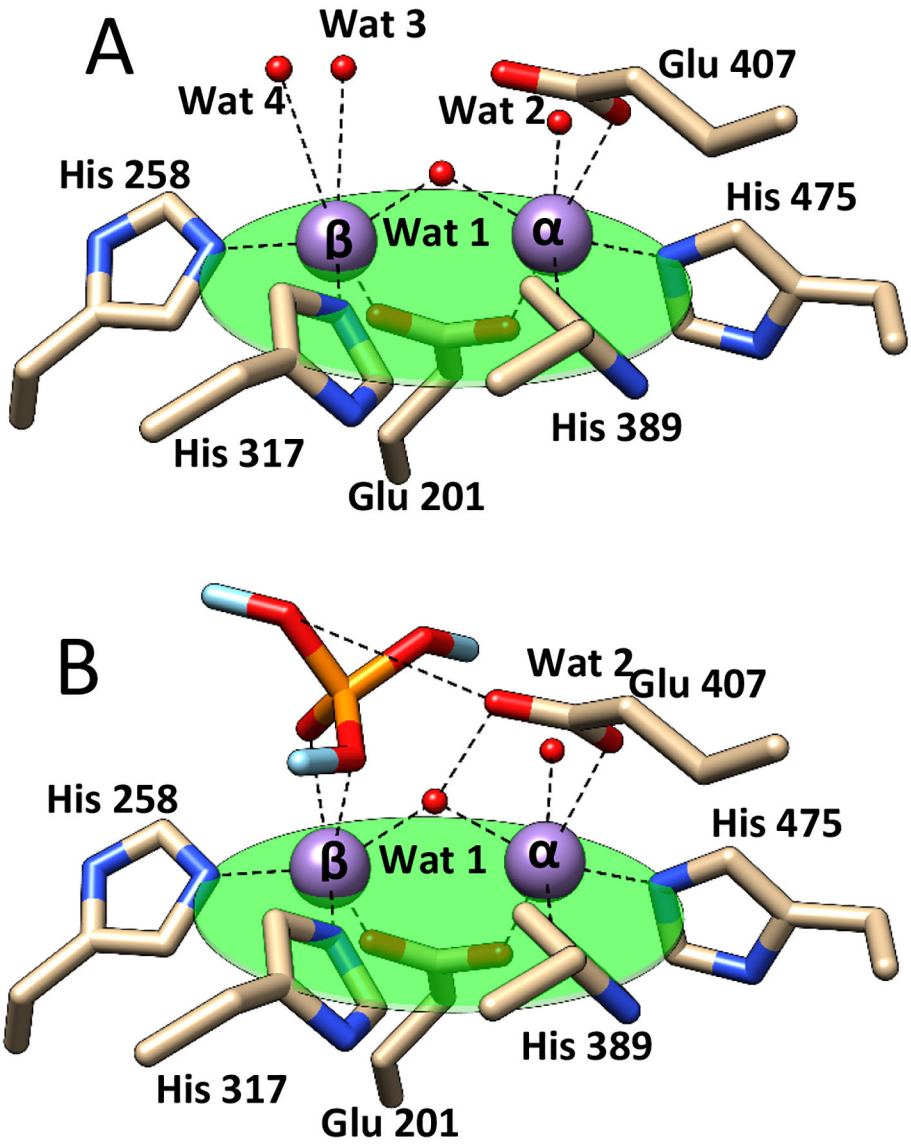

Figure 6.

Metal center of *Sb*-PTE. Green oval is the plane of the metal center defined by the coordinating nitrogens from the four histidine ligands. (A) apo metal center as found in the crystal structure. (B) proposed binding orientation of a generic phosphotriester.

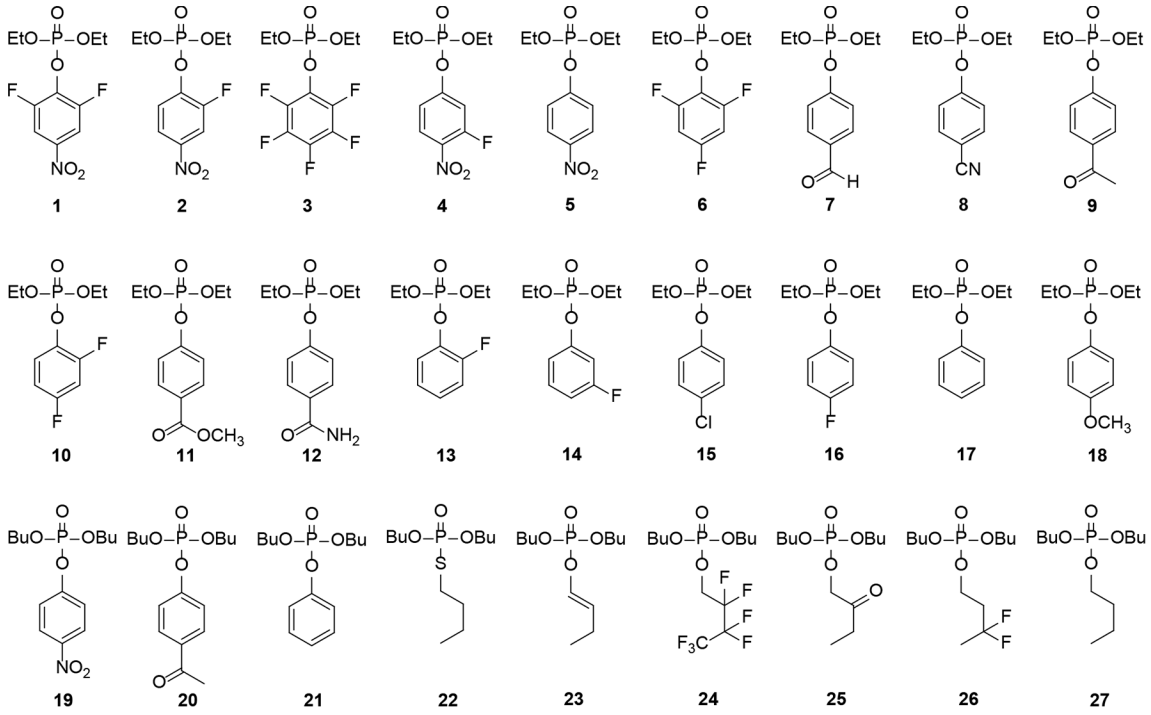

Scheme 1:
Structures of organophosphate triesters used as substrates for Sb-PTE.

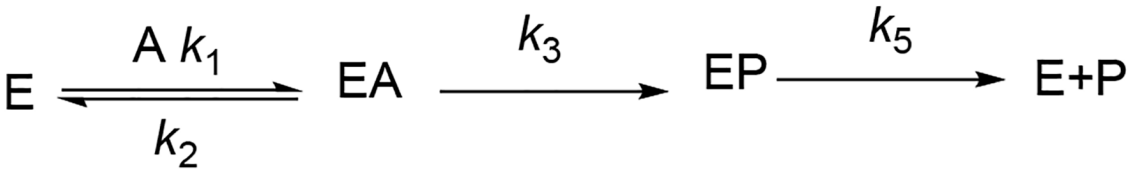

Scheme 2.

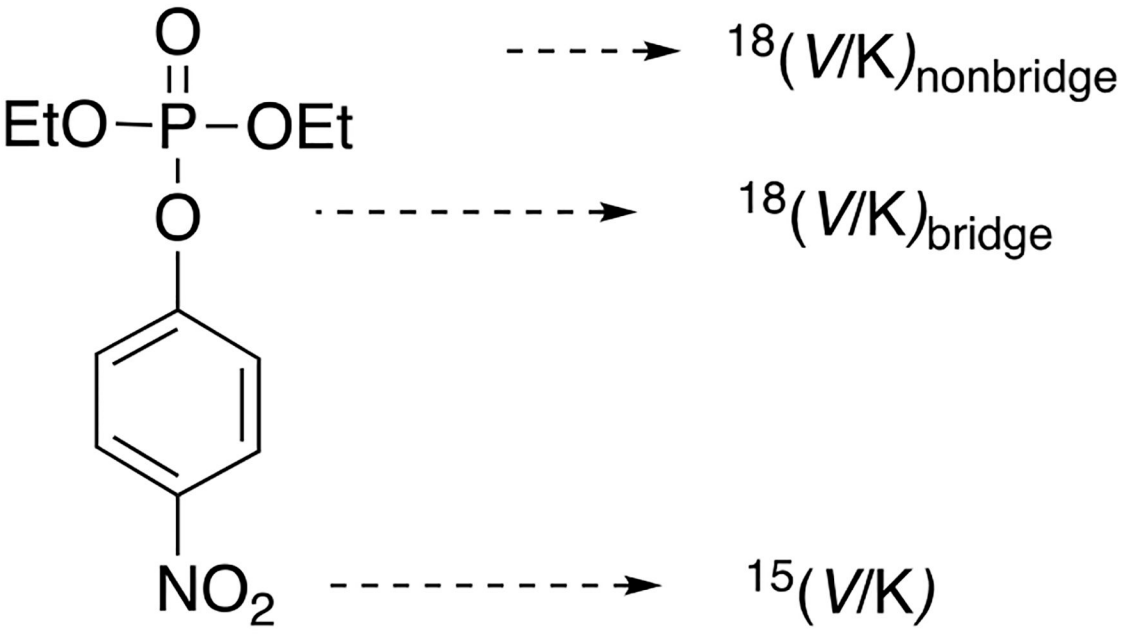

Scheme 3:
Sites on the paraoxon substrate where kinetic isotope effects were measured and their designations.

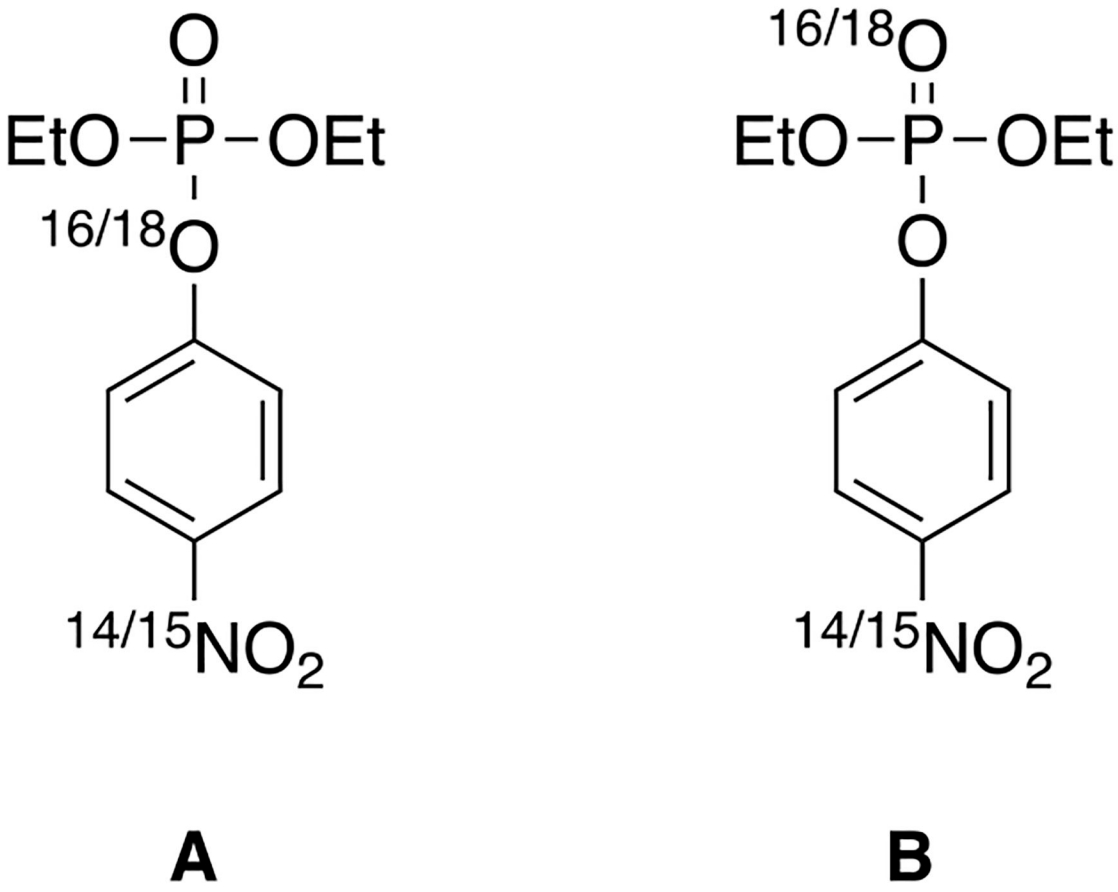

Scheme 4:

(A) The mixture of isotopic isomers of paraoxon used for measurement of $^{18}(k_{cat}/K_m)_{bridge}$. (B), the mixture of isotopic isomers of paraoxon used for measurement of $^{18}(k_{cat}/K_m)_{nonbridge}$.

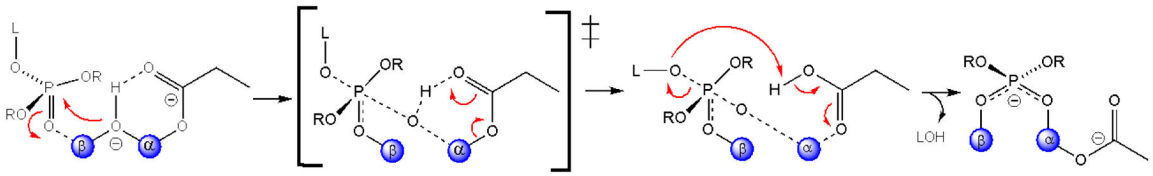

Scheme 5.
The proposed catalytic reaction mechanism for *Sb*-PTE.

Table 1.

Kinetics constant for the hydrolysis of phosphotriesters by *Sb*-PTE.

compound	pK_a [a]	F [b]	K_m (mM)	$^1k_{cat}$ (s^{-1})	$^1(k_{cat}/K_m)$ (M^{-1} s^{-1})	$^2k_{cat}$ (s^{-1})	$^2(k_{cat}/K_m)$ (M^{-1} s^{-1})	$^Tk_{cat}$ (s^{-1})	$^T(k_{cat}/K_m)$ (M^{-1} s^{-1})
1	4.10	1.00	1.10	93	8.5×10^4	-	-	93	8.5×10^4
2	5.45	0.95	0.63	38	5.9×10^4	1.8	2.9×10^3	40	6.2×10^4
3	5.53	1.00	0.46	167	3.6×10^5	-	-	167	3.6×10^5
4	5.94	0.98	0.25	105	4.2×10^5	2.1	8.0×10^3	107	4.3×10^5
5	7.14	0.93	0.32	30	9.5×10^4	2.4	7.2×10^3	32	1.0×10^5
6	7.38	0.95	0.95	68	7.2×10^4	2.8	3.8×10^3	71	7.6×10^4
7	7.66	0.57	1.20	18	1.5×10^4	13	1.1×10^4	31	2.6×10^4
8	7.95	0.84	0.67	78	1.2×10^5	15	2.2×10^4	93	1.4×10^5
9	8.05	0.49	0.24	0.26	1.1×10^3	0.26	1.1×10^3	0.6	2.2×10^3
10	8.43	0.75	0.39	9.5	2.4×10^4	3.2	8.2×10^3	13	3.3×10^4
11	8.47	0.53	1.00	1.7	1.7×10^3	1.5	1.5×10^3	3.2	3.2×10^3
12	8.56	0.20	0.55	0.2	2.7×10^2	0.60	1.1×10^3	0.8	1.4×10^3
13	8.81	0.87	1.30	18	1.4×10^4	2.7	2.1×10^3	21	1.6×10^4
14	9.28	0.53	0.27	43	1.6×10^5	38	1.4×10^5	81	3.0×10^5
15	9.38	0.03	0.41	1.2	2.9×10^3	39	9.5×10^4	40	9.8×10^4
16	9.91	0.08	1.60	5.9	3.7×10^3	72	4.5×10^4	78	4.9×10^4
17	10.04	0.23	1.10	16	1.5×10^4	55	5.0×10^4	71	6.5×10^4
18	10.29	0.16	0.44	0.38	8.6×10^2	2.1	4.6×10^3	2.5	5.5×10^3
19	7.14	0.78	0.15	5.9	3.9×10^4	1.6	1.1×10^4	7.5	5.0×10^4
20	8.05	0.87	0.43	2.2	5.1×10^3	0.3	7.1×10^2	2.5	5.8×10^3
21	10.04	0.85	0.14	3.7	2.6×10^4	0.7	4.7×10^3	4.4	3.1×10^4
22	10.78	0.80	0.085	0.34	4.0×10^3	0.08	9.1×10^2	0.42	4.9×10^3
23	11.1	0.58	0.088	0.48	5.5×10^3	0.35	4.0×10^3	0.83	9.4×10^3
24	12.5	0.31	0.11	0.11	1.0×10^3	0.25	2.3×10^3	0.36	3.3×10^3
25	13.0	0.95	0.05	0.043	8.6×10^2	0.002	4.9×10^1	0.045	9.1×10^2
26	13.9	0.26	0.17	0.033	1.9×10^2	0.010	5.7×10^2	0.043	7.6×10^2
27	16.1	0.33 [c]	nd	nd	1.0×10^1	nd	2.6×10^1	nd	3.9×10^1

[a] pK_a for compounds **1–21** were obtained from references[12, 14, 19] and[22]. pK_a values for compounds **22–26** were predicted values calculated with Advanced Chemistry Development (ACD/Labs) Software V11.02 and published by SciFinder. pK_a valued for compound **27** was taken from reference[23].

[b] F is fraction of most activated leaving group hydrolyzed as measured by ^{31}P NMR spectroscopy.

[c] Fractional values for **27** were calculated by dividing total observed hydrolysis by a factor of 3. The standard errors for the reported rate constants are less than ±15%.

Table 2.

Heavy atom isotope effects for the alkaline and enzymatic cleavage of phosphotriesters.

	^{15}N	$^{18}O_{bridge}$	$^{18}O_{nonbridge}$
alkaline hydrolysis	1.0007 ± 0.0001[a]	1.0060[b]	1.0063 ± 0.0001[b]
Sb-PTE (paraoxon)	1.0009 ± 0.0002	1.0102 ± 0.0006	1.0036 ± 0.0020
Pd-PTE (paraoxon)		1.0020[b]	1.0021 ± 0.0004[b]
Pd-PTE (compound **12**)		1.036 ± 0.002[b]	1.0181 ± 0.0007[b]

[a]Data from reference 24.

[b]Data from reference 19.